

# A new global dataset of mountain glacier centerline and length

Dahong Zhang <sup>1,2</sup>, Gang Zhou <sup>1,2</sup>, Wen Li <sup>1,2</sup>, Shiqiang Zhang <sup>1,2</sup>, Xiaojun Yao <sup>3</sup>, Shimei Wei <sup>3</sup>

<sup>1</sup> College of Urban and Environmental Science, Northwest University, Xi'an 710127, PR China

<sup>2</sup> Shaanxi Key Laboratory of Earth Surface System and Environmental Carrying Capacity, Northwest University, Xi'an 710127, PR China

<sup>3</sup> College of Geography and Environment Sciences, Northwest Normal University, Lanzhou 730070, PR China

*Correspondence:* Shiqiang Zhang (zhangsq@lzb.ac.cn)

**Abstract.** Length is one of the key determinants of glacier geometry and is an important parameter of glacier inventory and modeling; glacier centerlines are crucial inputs for many glaciological applications. In this study, the centerlines and maximum lengths of global glaciers were extracted using an automatic extraction algorithm based on the latest global glacier inventory data, digital elevation data (DEM), and European allocation theory. The glacier polygons were reconstructed according to the geometric principle and an automatic checking algorithm for the global glacier outlines was designed to filter erroneous or unsupported glacier outlines. The DEMs of global glacier-covered regions were compiled using available DEMs. An updated automatic extraction tool was designed independently, and a parameterization scheme with empirical thresholds was applied for data production. The accuracy of the dataset was evaluated using random assessment with visible interpretation and comparative analysis with another dataset. The 10,764 erroneous glacier polygons, 7,174 ice caps, and 419 nominal glaciers from the Randolph Glacier Inventory (RGI) version 6.0 were identified and excluded, accounting for 8.25% of the total. In total, 198,137 glacier centerlines were generated, accounting for 99.74% of the total input glaciers and 91.52% of the RGI v6.0. The accuracy of glacier centerlines was 89.68%. The comparison between the dataset and previous datasets suggested that the majority of glacier centerlines were slightly longer than those in RGI v6.0. The extraction method of this study has a strong ability to obtain the maximum length of glaciers, meaning that the maximum lengths of some glaciers were likely underestimated in the past. The dataset constructed includes 17 sub-datasets, such as the global glacier centerline dataset, global glacier maximum length dataset, and global glacier DEM dataset, all of which can be found at link: <https://doi.org/10.11922/sciencedb.01643> (Zhang and Zhang, 2022).

## 1 Introduction

Mountain glaciers which are distinct from the Greenland and Antarctic ice sheets, are also shrinking rapidly (Hugonnet et al., 2021). They are altering regional hydrology (Pritchard, 2019), raising global sea levels (Cazenave, 2018), and elevating natural hazards (Shukla and Sen, 2021; Zheng et al., 2021). These glaciers are among the most climate-sensitive constituents of the world's natural water towers (Immerzeel et al., 2019). Under the influence of global climate change, studies on glacier area changes (Sommer et al., 2020; Li et al., 2021), ice thickness (Farinotti et al., 2019), mass balance (Zemp et al., 2019; Vargo et al., 2020; Wu et al., 2021), ice velocity field (Thogersen et al., 2019), the impact of debris-cover (Scherler et al., 2018; Shukla et al., 2020; Herreid and Pellicciotti, 2020), glacier meltwater (Noel et al., 2020), sediment release (Aciego et al., 2015; Li et al., 2019), and related hazards (Zhou et al., 2021b; Stuart-Smith et al., 2021; Käab et al., 2021) in glacier-covered regions are essential for global water resources supply and disaster prevention and reduction.

44

45 The most obvious distinction between glaciers and other natural ice bodies is their property to move  
46 towards lower altitudes under the influence of gravity. Glacier flow lines are the motion trajectories  
47 of a glacier and the main flow line is the key trajectory. The main flow line cannot be obtained on a  
48 large scale owing to the lack of glacier velocity field data. The glacier centerline, generated via the  
49 axis line method (Le Bris and Paul, 2013; Machguth and Huss, 2014; Kienholz et al., 2014; Zhang  
50 et al., 2021), is typically used to represent the main flow line. The glacier centerline is a critical  
51 parameter for analyzing the ice velocity field (Heid and Kääb, 2012; Melkonian et al., 2017),  
52 estimating the glacier volume (Li et al., 2012; Gao et al., 2018), and developing glacier models  
53 (Oerlemans, 1997; Sugiyama et al., 2007; Maussion et al., 2019).

54

55 Glacier length, usually referring to the maximum length of a glacier centerline (main flow line),  
56 represents the longest motion trajectory of a glacier, which is one of the key determinants of glacier  
57 geometry and a basic parameter of glacier inventories (RGI Consortium, 2017) and modeling  
58 (Maussion et al., 2019). Glacier length fluctuations can be used to quantify glacier changes (Zhou  
59 et al., 2021a), such as by identifying glacier advancement, surge, or retreat. Glacier length  
60 fluctuations (e.g., Leclercq et al., 2014) have also been used to study the relationships with changes  
61 in glacier area (Winsvold et al., 2014) and the geometric structure of a glacier (Herla et al., 2017),  
62 estimate glacier volume in combination with the glacier area (Lüthi et al., 2010), and reconstruct  
63 annual averaged surface temperatures over the past 400 years on hemispherical and global scales  
64 (Leclercq and Oerlemans, 2011).

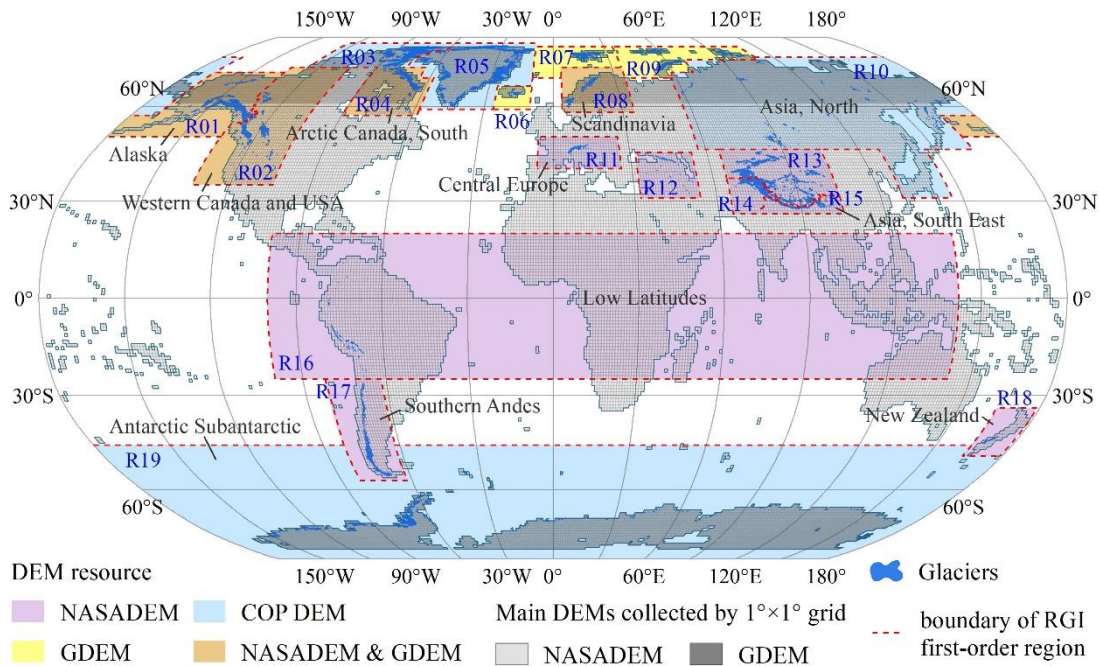
65

66 The global complete inventory (RGI Consortium, 2017) of glacier outlines was created following  
67 the Fifth Assessment Report of the Intergovernmental Panel on Climate Change (IPCC AR5). To  
68 meet the demand for large-scale acquisition of glacier length, automatic and semi-automatic  
69 methods have been proposed. There are three types of methods: first, the typical hydrological  
70 analysis method (Schiefer et al., 2008), but the lengths are longer than equivalent maximum  
71 distances taken along typical longitudinal centerline profiles; second, a simplified algorithm based  
72 on skeleton theory (Le Moine and Gsell, 2015), but this method has not been widely used; third,  
73 centerline method based on the axis concept, proposed by Le Bris and Paul (2013), and applied to  
74 the calculation of global glacier length for the first time by Machguth and Huss (2014). However, it  
75 is difficult to extract complex glaciers using the method (Le Bris and Paul, 2013). The cost grid-  
76 least-cost route approach of Kienholz et al. (2014) based on the axis concept has higher accuracy,  
77 but it requires more labor and time, which limits its application to global glaciers. The trade-off  
78 function approach of Machguth and Huss (2014) was based on the axis concept, their results cover  
79 almost all mountain glaciers in the world but exclude the centerlines of branches of glaciers.  
80 Therefore, researchers have been trying to overcome these difficulties in recent years (Yao et al.,  
81 2015; Yang et al., 2016; Ji et al., 2017; Hansen et al., 2020; Xia, 2020; Zhang et al., 2021). To date,  
82 global datasets of the centerline and length of mountain glaciers are rare, including that of glacier  
83 branches. Based on our recent study (Zhang et al., 2021) on successfully extracting the glacier  
84 centerline using the Euclidean allocation, in this study, we aim to combine free, available digital  
85 elevation data into one global digital elevation model (DEM) with 30 m resolution from 90°N to  
86 90°S, check and correct the global glacier outlines, and obtain a new graphic dataset of the centerline  
87 and length for global mountain glaciers based on the updated DEM and outlines.

88

## 89 2 Study region and data

90 The glacier dataset used in this study was the RGI version 6.0  
 91 (<http://www.glims.org/RGI/randolph.html>, last accessed: 15 November 2021) released via the  
 92 Global Land Ice Measurements from Space initiative (GLIMS), which is a globally complete  
 93 collection of digital outlines of glaciers, excluding ice sheets (Pfeffer et al., 2014). RGI v6.0 includes  
 94 216,502 glaciers (215,547 glaciers described in the product handbook) worldwide, with a total area  
 95 of 705,738.793 km<sup>2</sup> (RGI Consortium, 2017). All glaciers can be divided into 19 first-order glacier  
 96 regions (Radić and Hock, 2010), and these regions were used in our study (Fig. 1).



97

98 **Figure 1.** Distribution of global glaciers, first-order glacier regions, and DEMs. The background is  
 99 the global DEM grid (1°×1°) covered by NASADEM and GDEM. GDEM and COP DEM represent  
 100 the ASTER GDEM v3 and the Copernicus DEM, respectively. **Notes:** R03: Arctic Canada, North;  
 101 R05: Greenland Periphery; R06: Iceland; R07: Svalbard and Jan Mayen; R09: Russian Arctic; R12:  
 102 Caucasus and Middle East; R13: Asia, Central; R14: Asia, South West.

103

104 Five DEM products (Table 1) were collected in preliminary studies. The National Aeronautics and  
 105 Space Administration (NASA) DEM (NASADEM) (<https://lpdaac.usgs.gov/news/release-nasadem-data-products/>, last accessed: November 17, 2021) was released by the Land Processes  
 106 Distributed Active Archive Center (LP DAAC) in January 2020. As a modernization of the DEM  
 107 and associated products generated from the Shuttle Radar Topography Mission (SRTM) data (Farr  
 108 et al., 2007), the NASADEM, with a low mean absolute error (MAE) (Carrera-Hernández, 2021),  
 109 is the successor of the NASA SRTM V3. The root mean square error (RMSE) of NASADEM is  
 110 smaller than that of SRTM (Uuemaa et al., 2020). Serving the zonal extent of (56°S, 61°N),  
 111 NASADEM was used as the preferred DEM in this study because of its superior performance. The  
 112 Advanced Spaceborne Thermal Emission and Reflection Radiometer (ASTER) is a 14-channel  
 113 imaging instrument operating on the Terra satellite of NASA since 1999. ASTER Global Digital  
 114 Elevation Model (GDEM) version 3 (<https://lpdaac.usgs.gov/news/nasa-and-meti-release-aster->

116 global-dem-version-3/, last accessed: November 17, 2021) (Abrams et al., 2020) was released by  
 117 Japan's Ministry of Economy, Trade, and Industry (METI) and NASA in July 2019. Using ICESat  
 118 data, Carabajal and Boy (2016) found that ASTER GDEM v3 displayed smaller means, similar  
 119 medians, and less scatter than ASTER GDEM v2 in Greenland and Antarctica. To determine the  
 120 zonal extent of (56°S, 83°S) and (61°N, 83°N), ASTER GDEM v3 was used as the second priority  
 121 DEM in this study.

122  
 123 NASADEM and ASTER GDEM v3 do not cover all glacierized regions, missing parts of the polar  
 124 region and the Kamchatka Peninsula. Because of their high temporal and spatial resolution at high  
 125 latitudes, the reference elevation model of Antarctica (REMA) (Howat et al., 2019) and ArcticDEM  
 126 (<https://www.pgc.umn.edu/data/arcticdem/>, last accessed: November 17, 2021) were preferred as  
 127 the supplementary data of our preliminary studies in these glacier regions. Nevertheless, ArcticDEM  
 128 and REMA are not suitable because of insufficient coverage and sporadic data. Therefore,  
 129 Copernicus DEM (<https://spacedata.copernicus.eu/web/cscda/cop-dem-faq>, last accessed:  
 130 November 17, 2021) with a wide coverage was finally determined as the supplementary data for  
 131 glacier regions not covered via the NASADEM and ASTER GDEM v3 completely. The Copernicus  
 132 DEM was recently released (November 2020) and the accuracy assessment undertaken by its  
 133 development team (the product handbook) using TanDEM-X DEM/World DEM ICESat GLAS  
 134 reference points found an absolute vertical accuracy of approximately 10 m at the periphery of  
 135 Antarctica and Greenland. Finally, NASADEM, ASTER GDEM v3, and Copernicus DEM were  
 136 compiled to create a 30 m DEM of the completely covered study area.

137 **Table 1.** All DEMs collected in this study

DEM	Extent	Resolution	Access
NASADEM	[56°S, 61°N]	30 m	<a href="https://search.earthdata.nasa.gov/search">https://search.earthdata.nasa.gov/search</a>
ASTER GDEM v3	[83°S, 83°N]	30 m	<a href="https://gdemdl.aster.jspacesystems.or.jp/">https://gdemdl.aster.jspacesystems.or.jp/</a>
ArcticDEM	[55°N, 90°N]	2 m	<a href="https://earthengine.google.com/">https://earthengine.google.com/</a>
REMA	[60°S, 88°S]	2m / 8m	<a href="https://earthengine.google.com/">https://earthengine.google.com/</a>
Copernicus DEM	Global	30 m	<a href="https://panda.copernicus.eu/web/cds-catalogue/panda">https://panda.copernicus.eu/web/cds-catalogue/panda</a>

138 **Note:** The interval in the 'Extent' column represents all landmasses within a zonal range, but coverage may not exist  
 139 for all areas.

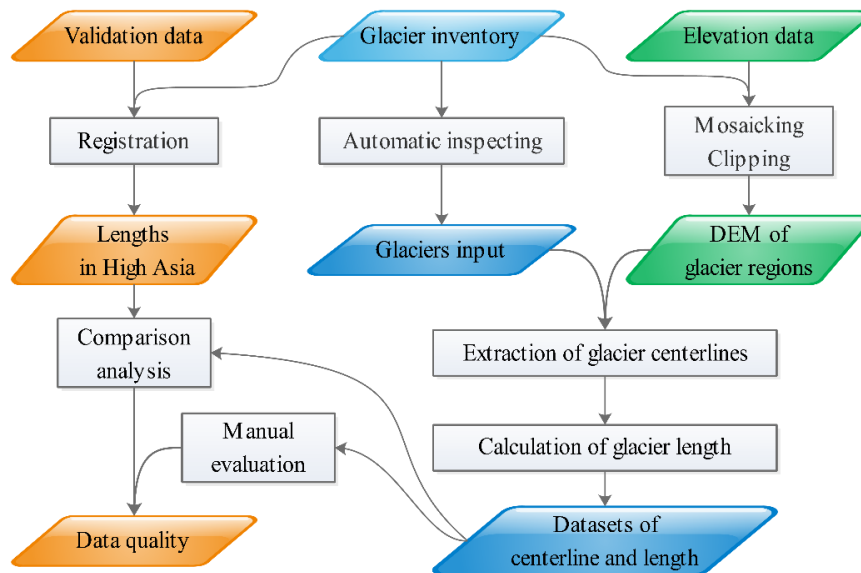
140  
 141 In addition, graphical data (Machguth and Huss, 2014) of glacier length in \*. xy format with an  
 142 unknown projection coordinate system in High Asia were collected, which correspond to the  
 143 attribute of the glacier maximum length ( $L_{max}$ ) in RGI v6.0. Because the data was obtained from an  
 144 unofficial source, we could not access the data description documents and only recovered the  
 145 coordinate matching between these points and some glaciers in RGI v6.0. Registration of the \*. xy  
 146 file depends on the match between its filename and the feature identity document (FID) of the glacier  
 147 polygon of RGI v6.0 in the same glacier area. The glacier lengths (*MHMLDS*) of successful  
 148 registration were used as graphical validation data for this study.

### 150 3 Methods

#### 151 3.1 Outline of workflow

152 This study relied on two key input datasets: global glacier inventory and compiled global glacier  
 153 elevation. The goal of this study was to establish a new dataset of global graphic glacier centerlines  
 154 and lengths. An outline of the workflow is shown in Figure 2. The process was divided into six parts:

155 (1) design an algorithm to check all glacier outlines, marks, and exclude defective glacier polygons;  
 156 (2) buffer glaciers to produce a mask containing global glaciers and their buffers; (3) mosaic  
 157 compiled global DEMs according to the masks in step 2 of different glacier regions to prepare the  
 158 global glacier elevation data; (4) determine the automatic extraction parameters of glacier  
 159 centerlines around the world by repeated testing in each region; (5) input the global DEM and glacier  
 160 outline dataset and all parameters into the designed automatic extraction software (Zhang et al.,  
 161 2021) to generate the centerlines and length in the global glacier; and (6) verify and compare with  
 162 other centerline results obtained via different methods to evaluate the accuracy of the new datasets.

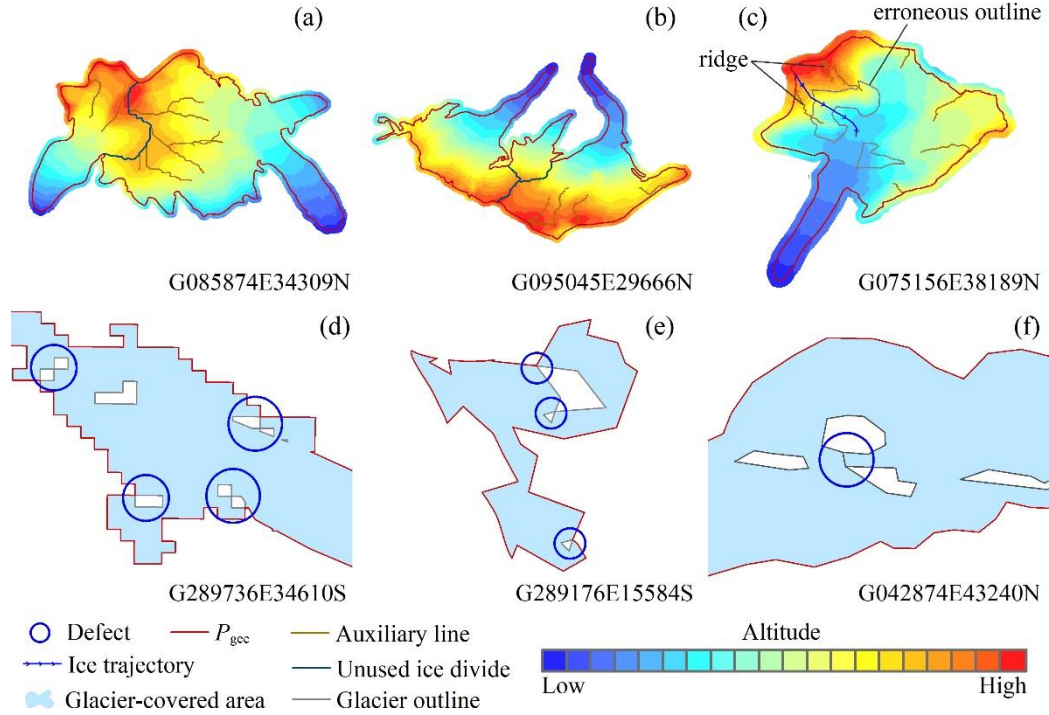


163  
 164 **Figure 2.** Workflow of the centerline and length dataset production.  
 165

### 166 3.2 Illustration of key methods

#### 167 3.2.1 Pre-process of glacier outlines

168 This study had strict requirements for glacier outlines, and all glacier complexes should be divided  
 169 into individual glaciers before centerline extraction. However, because of the limited semi-  
 170 automatic glacier segmentation approach (Kienholz et al., 2013) and the high-priority strategy of  
 171 completeness of coverage adopted by RGI v6.0 (RGI Consortium, 2017), some glaciers were not  
 172 supported by our algorithm. These glaciers included three categories: glacier complexes  
 173 with/without inaccurate segmentation (Fig. 3a-b), incorrect glacier outlines (Fig. 3c), and flawed  
 174 glaciers (Fig. 3d-f) generated by the automatic extraction algorithm. For the third category, we  
 175 designed an identification algorithm (see paragraph 3) to mark and screen them. The flaws in these  
 176 glacier outlines were mainly caused by topology errors of polylines/polygons, such as unclosed,  
 177 sawtooth, and overlap. The first two categories do not affect the program's normal operation;  
 178 however, the accuracy of the extraction results is difficult to guarantee. We cannot identify them at  
 179 present and a solution is needed to improve the quality of the global glacier inventory.



180

181 **Figure 3.** Schematic of three types of flawed glacier outlines. **(a-b)** Glacier complexes with/without  
 182 inaccurate segmentation. **(c)** Incorrect glacier outline. **(d-f)** Panels represent three common  
 183 problems in flawed glaciers: defects in automatic algorithm, defects in post-processing, and artificial  
 184 errors. Auxiliary line represents lower-grade ice divide in the individual glacier, which is part of the  
 185 ridge lines.

186

187 In this study, we defined the external contour of a glacier ( $P_{gcc}$ ), namely, the polygon corresponding  
 188 to the longest closed polyline of the glacier, to reduce the storage of DEMs and improve the  
 189 efficiency of batch processing. The buffer masks of all glaciers (buffer distance: approximately 100  
 190 m) were generated by their  $P_{gcc}$  to meet the requirement for the extent of input DEMs to be slightly  
 191 larger than the  $P_{gcc}$ . The buffer masks generated initially were relatively broken because there are  
 192 overlaps or gaps between the adjacent polygons of the buffer zone. We merged small spots to remove  
 193 polygons with a perimeter less than 12 times the buffer distance on the glacier buffer masks of each  
 194 region.

195

196 The third category of glaciers (Fig. 3d-f) with flaws was identified by obtaining  $P_{gcc}$ . In the third  
 197 category, the most common type is two or more closed polylines with the same endpoint in a glacier.  
 198 There were also a few glacier polygons with false closed polylines, which are the head and tail  
 199 endpoints of the polylines that do not coincide, but the distance is less than the tolerance. The  
 200 solution are as follows: flawed glacier outlines were identified by judging whether there were  
 201 multiple polylines sharing endpoints after converting the glacier from a polygon to polylines, but  
 202 these outlines do not include the false closed type.

203

### 204 3.2.2 Preparation of input datasets

205 All data were processed in units of first-order glacier regions. The input glacier outlines excluded  
 206 all the defective glacier outlines. Similarly, the nominal glaciers (represented by an ellipse) and ice

207 caps remarked in RGI v6.0 were also treated, which were distinguished by two attributes: status  
 208 (nominal glacier) and form (ice cap). The inspection results (Table 2) of glacier outlines show that  
 209 there are 10,764 defective glacier outlines (*FGODS*) in RGI v6.0, accounting for approximately  
 210 4.97% of the total (216,502). After excluding nominal glaciers (461) and ice caps (7,174), 198,646  
 211 glaciers remained as input glacier outlines (*IGODS*), accounting for 91.75% of the global mountain  
 212 glaciers.

213 **Table 2.** Preprocessing results of different glacier regions and information of input datasets.

Region	Region Name	Total	Ice Cap	Nominal glacier	Flawed glacier	Glacier input	DEM input
R01	Alaska	27108	0	0	704	26404	NASADEM, GDEM
R02	Western Canada and USA	18855	0	0	1564	17291	NASADEM, GDEM
R03	Arctic Canada, North	4556	650	0	47	3869	COP DEM
R04	Arctic Canada, South	7415	953	0	63	6409	NASADEM, GDEM
R05	Greenland Periphery	20261	1658	0	1547	17247	COP DEM
R06	Iceland	568	133	0	1	435	GDEM
R07	Svalbard	1615	144	0	12	1460	GDEM
R08	Scandinavia	3417	0	4	75	3338	NASADEM, GDEM
R09	Russian Arctic	1069	460	0	0	609	GDEM
R10	North Asia	5151	5	116	136	4899	COP DEM
R11	Central Europe	3927	0	2	76	3849	NASADEM
R12	Caucasus Middle East	1888	0	339	2	1547	NASADEM
R13	Central Asia	54429	1545	0	28	52858	NASADEM
R14	South Asia West	27988	295	0	1946	25792	NASADEM
R15	South Asia East	13119	289	0	4	12826	NASADEM
R16	Low Latitudes	2939	0	0	724	2215	NASADEM
R17	Southern Andes	15908	623	0	3828	11734	NASADEM
R18	New Zealand	3537	0	0	0	3537	NASADEM
R19	Antarctic Subantarctic	2752	419	0	7	2327	COP DEM
--	--	216502	7174	461	10764	198646	--

214 **Note:** GDEM and COP DEM represent ASTER GDEM v3 and Copernicus DEM, respectively.

215  
 216  $P_{\text{gec}}$  of all glaciers in RGI v6.0 constitute the global glacier external contour dataset (*GGECDS*),  
 217 which generated the buffer mask dataset (*GGBMDS*) of global mountain glaciers. The collected  
 218 DEMs were extracted using *GGBMDS* and 43,035 DEM tiles were generated. They were then  
 219 mosaicked according to different first-order glacier regions to generate a global glacier elevation  
 220 dataset (*GGEDS*). The details of the two input datasets are presented in Table 2.

### 222 3.2.3 Generation of centerline and glacier length

223 The automatic extraction tool of ‘GlacierCenterlines\_Py27’ (Update to version 5.2.1) was used,  
 224 which is based on the axis concept and Euclidean allocation (Zhang et al., 2021). The principle is  
 225 briefly explained as follows: the highest and lowest points of the external outline of a glacier as two  
 226 endpoints were extracted, cells with the equal shortest distances from the cell to both sides were  
 227 identified in a glacier polygon, and the line formed by these cells was regarded as the glacier  
 228 centerline. The maximum length of glaciers was calculated using an algorithm similar to the critical  
 229 path. The updated contents focused on formulating the parameterization scheme (Appendix A: Table  
 230 A1) for extracting global glacier centerlines, as well as repairing some newly discovered bugs, such  
 231 as a dead cycle in the process of auxiliary line extraction. All glacier outlines included in the *IGODS*  
 232 were divided into ten levels (Table 3) using the proportion of cumulative area after ranking the area  
 233 of all input glacier polygons from small to large. User-defined Albers with WGS1984 as the



234 reference ellipsoid were used as a unified projection coordinate system. The central meridian,  
 235 standard parallel 1, standard parallel 2, and origin latitude of the different glacier regions were  
 236 determined by their spatial extent. The empirical values of the other parameters were determined in  
 237 repeated attempts and their values had a significant correlation with glacier scale. The glacier  
 238 centerlines generated were merged according to the glacier regions and the graphics and attribute  
 239 information of glacier length were exported as corresponding independent ESRI shapefiles. In  
 240 addition, some key associated data were exported, such as the segmentation results of glacier  
 241 outlines, the lengths in the accumulation and ablation region of each glacier, the lowest points, the  
 242 local highest points ( $P_{max}$ ), the failed glacier outlines dealt, and logs.

243

**Table 3.** Statistics of global glaciers by different levels.

Level	Count	Area/km <sup>2</sup>	Acc. area/km <sup>2</sup>	Percent	Interval/km <sup>2</sup>
L1	165593	1.00	41313.79	10%	[0.01, 1.00]
L2	22833	3.57	82629.47	20%	(1.00, 3.57]
L3	6906	11.39	123947.69	30%	(3.57, 11.39]
L4	2149	35.51	165282.14	40%	(11.39, 35.51]
L5	698	103.10	206631.32	50%	(35.51, 103.10]
L6	262	248.26	247917.55	60%	(103.10, 248.26]
L7	113	521.40	289227.71	70%	(248.26, 521.40]
L8	55	1087.47	330595.34	80%	(521.40, 1087.47]
L9	27	2657.74	374312.14	90%	(1087.47, 2657.74]
L10	10	6004.85	413136.71	100%	(2657.74, 6004.85]
Total	198646	--	--	--	--

244

### 245 3.2.4 Accuracy assessment

246 A random assessment was prioritized in this study. We randomly selected 100 glaciers in each  
 247 glacier region and obtained 19 samples with a total of 1,900 glacier centerlines. These glacier  
 248 centerlines were divided by artificial inspection into three first-level categories (Zhang et al., 2021):  
 249 correct (I), inaccurate (II), and incorrect (III). Type II mostly contains glaciers with accurate glacier  
 250 maximum lengths but missing, redundant, or unreasonable branches of glacier centerlines. When  
 251 calculating verification accuracy, Types I and II were regarded as correct, and only Type III was  
 252 considered incorrect. Finally, the glacier proportion of Type III in the sample was counted and the  
 253 valuation result ( $R$ ) was calculated using Eq. (1).

$$254 \quad R = \sum_{i=1}^{19} \frac{S_i \times N_{T_i}}{N_G} \quad , (1)$$

255 where  $N_G$  is the total quantity of glaciers and  $N_{T_i}$  and  $S_i$  are the verification accuracy and number of  
 256 glaciers in the corresponding glacier region of the  $i$  th sample ( $i = 1, 2, 3, \dots, 18, 19$ ), respectively.  
 257 All glacier maximum lengths ( $G_{L_{max}}$ ) in this study were compared with the  $L_{max}$  (Machguth and  
 258 Huss, 2014) in RGI v6.0 using linear correlation and ratio analysis. Here, we took  $L_4 - L_{10}$  at the  
 259 glacier level as the same grade for statistics. The correlations between  $G_{L_{max}}$  and  $L_{max}$  were  
 260 established according to different glacier regions and glacier levels and the length ratio,  $R_r$  (Eq. 2),  
 261 was calculated. In addition, considering the differences between the graphics, we also collected  
 262 graph data of glacier length extracted by Machguth and Huss (2014). Considering the limited  
 263 availability of data (obtained: R13–R15), we only compared two glacier-covered regions in the  
 264 Himalayas: Mount Qomolangma and Kangchenjunga (the world's third-highest mountain) and their  
 265 surrounding areas.



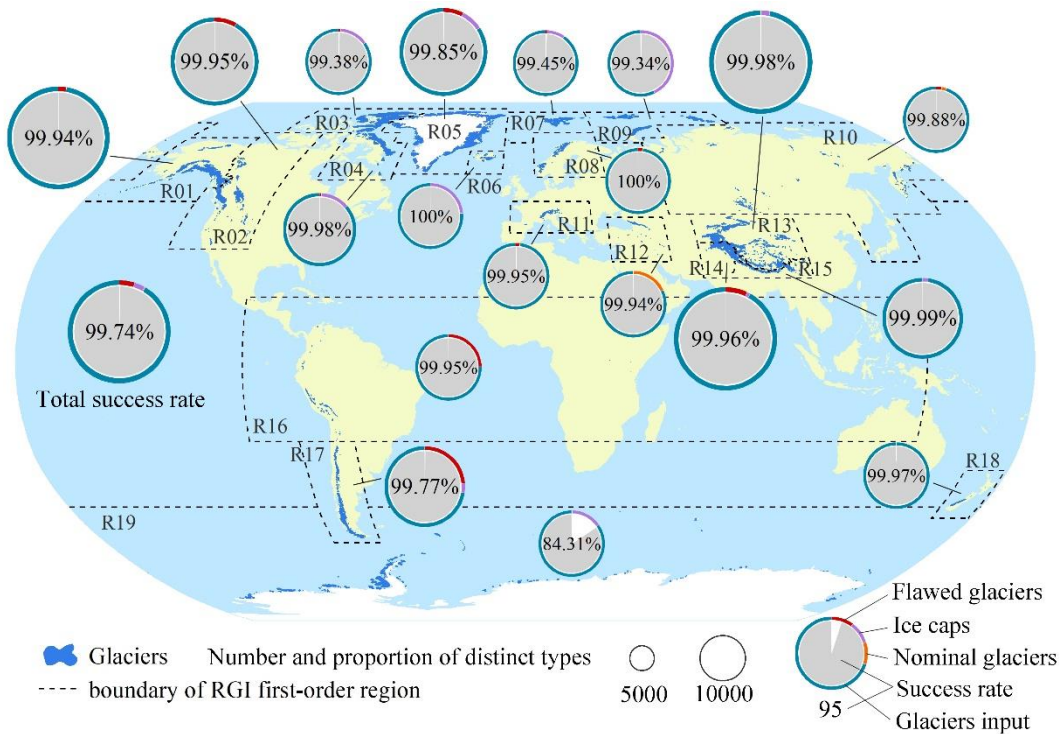
266 
$$R_r = \frac{G_{L_{\max}}}{L_{\max}} \quad (2)$$

267

268 **4 Results**

269 **4.1 Centerline and length of glaciers**

270 Taking the *IGODS*, *GGEDS*, and other model parameters as input data, 198,137 glacier centerlines  
 271 were automatically generated using the centerline extraction tool of 'GlacierCenterlines\_Py27  
 272 v5.2.1', with an overall success rate of 99.74%. The number and proportion of flawed glacier  
 273 outlines, nominal glaciers, ice caps, input glacier outlines, and extraction results for distinct glacier  
 274 regions are shown in Fig. 4.



275

276 **Figure 4.** Extraction results of glacier centerlines in different glacier regions. The ring in the pie  
 277 chart represents the proportion of input glacier number and the number of excluded three glacier  
 278 types with total number of glaciers in the region. Pie chart represents the correct rate, which is the  
 279 proportion of the extraction result number with input glacier quantity. The size of the pie/ring  
 280 represents the grade of the glacier number in the region.

281

282 Except for Antarctica and Subantarctica (R19), the success rates of extracting glacier centerlines in  
 283 other glacier regions were greater than 99%, which indicates that the automatic extraction algorithm  
 284 for glacier centerlines is robust. A small number of glacier outlines with false closed problems and  
 285 unidentified ice caps were the main reasons for the failure of automatic extraction of glacier  
 286 centerlines; however, it is difficult to establish rules for accurately identifying these glacier polygons.  
 287 In total, 510 unsuccessful glacier outlines were identified, of which Antarctic-Subantarctic (R19)  
 288 accounted for 71.57%; Southern Andes (R17) and Greenland Periphery (R05) for 5.29% and 5.1%,  
 289 respectively; Arctic Canada North (R03) and Alaska (R01) for 4.71% and 2.94%, respectively; and  
 290 other glacier regions for less than 2%.

291

292 Overall, the global glacier centerline dataset (*GGCLDS*) constructed in this study contained 91.52%  
 293 of the total glaciers in RGI v6.0. The lengths of each branch of the glacier centerline were derived  
 294 and the longest branch lengths of the glacier centerline were defined as the glacier maximum length  
 295 ( $G_{Lmax}$ ), which were used to form the global glacier maximum length dataset (*GGMLDS*). The  
 296 average centerline length of all branches of a glacier is called the glacier mean length ( $G_{Lmean}$ ). In  
 297 addition, the median glacier altitude was regarded as the equilibrium line altitude (ELA) (Machguth  
 298 and Huss, 2014), the part with  $G_{Lmax}$  higher than ELA was regarded as the length of the glacier  
 299 accumulation zone ( $G_{Lacc}$ ), and the part lower than ELA was regarded as the length of the glacier  
 300 ablation zone ( $G_{Labl}$ ), which formed the glacier accumulation zonal length dataset (*GACLDS*) and  
 301 glacier ablation zone length dataset (*GABLDS*). The key process data corresponding to *GGCLDS*  
 302 were also output, to form the glacier outline segmentation results (*GOSRDS*), lowest points  
 303 (*GGLPDS*), local highest points (*GLHPDS*), and unsuccessful glacier outlines (*GUGODS*). The  
 304 fields involved in all datasets are explained in Table 4.

305

**Table 4.** Description of the attributes contained in all datasets.

Name	Data type	Char. length	Description
GLIMS_ID	Char.	14	Unique code of a glacier
Type	Long int.	4	Glacier grade in this study
MaxL	Float	8	Glacier maximum length (Unit: m)
MeanL	Float	8	Glacier average length (Unit: m)
ELA	Long int.	4	Equilibrium line altitude (Unit: m)
AccL	Float	8	Length in the accumulation region (Unit: m)
AblationL	Float	8	Length in the ablation region (Unit: m)
Id	Long int.	8	Data code of the same glacier
BS	Long int.	8	Tag of the same segment in a glacier
RASTERVALU	Long int.	4	Altitude of a $P_{max}$ (Unit: m)

306

**Note:** Char. and int. represent Character and integer, respectively.

307

308 The glacier outlines of RGI v6.0 without centerline results in this study were limited by the quality  
 309 of the glacier polygons, which mainly correspond to the flawed glacier outlines (*FGODS*), and the  
 310 identified ice caps in RGI v6.0 (Table 2). Among the *FGODS* (10,764), Southern Andes (R17) had  
 311 the most, followed by Southwest Asia (R14); Western Canada and USA (R02) and Greenland  
 312 Periphery (R05), with slightly more than 1,500; and Low Latitudes (R16) and Alaska (R01), with  
 313 slightly more than 700. There were 451 in other glacier regions, including two regions with 0  
 314 defective glacier outline, the Russian Arctic (R09) and New Zealand (R18). Among the ice caps  
 315 (7174) identified by RGI v6.0, slightly more than 1,500 were in R05 and Central Asia (R13),  
 316 between 500 and 1,000 in the Arctic Canada South (R04), Arctic Canada North (R03), and R17, and  
 317 less than 500 in other glacier regions. Nominal glaciers (461) existed in three glacial regions:  
 318 Caucasus Middle East (R12), North Asia (R10), and Scandinavia (R08).

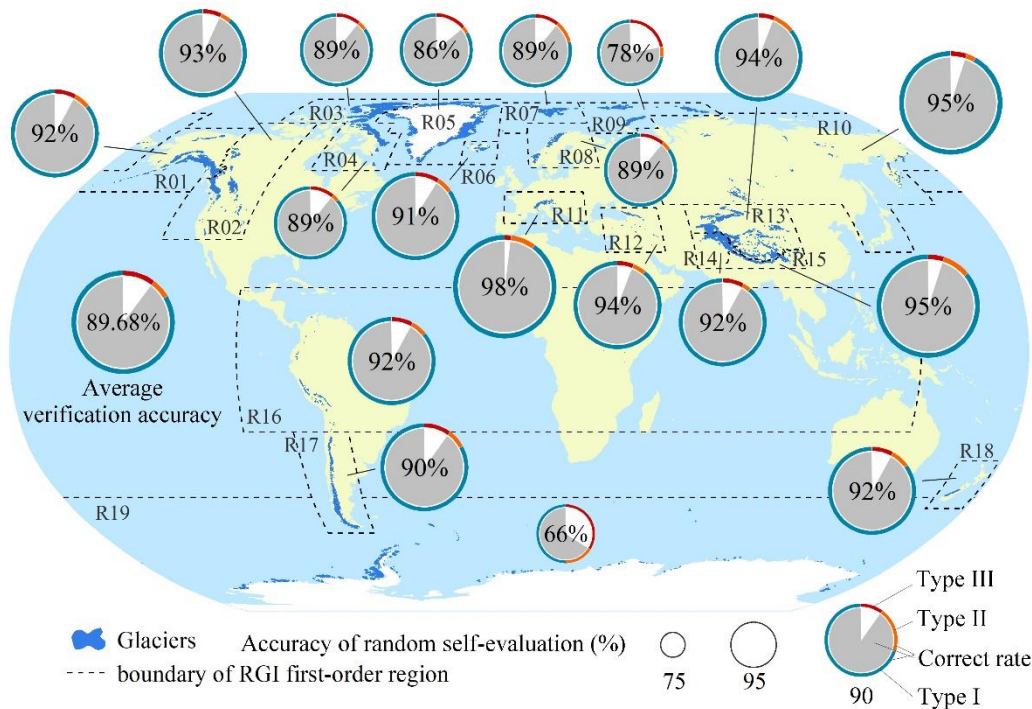
319

## 320 4.2 Data validation

### 321 4.2.1 Random self-assessment results

322 The evaluation results using random samples from the glacier centerline dataset suggested that the  
 323 average verification accuracy of the glacier centerline dataset was 89.68%. There were significant  
 324 differences in the accuracy of the 19 glacier regions around the world (Fig. 5). Among them, R11,  
 325 R15 and R10, R09, and R19 were the highest (98%), second highest (95%), slowest lower (78%),  
 326 and lowest (50%), respectively. In terms of types, the average proportions of Types I and II were

327 83.53% and 6.16%, respectively. The proportion of Type I in R07 and R09 was relatively low, at  
 328 79% and 73%, respectively, and the lowest in R19 was only 50%. Type II had the highest proportion  
 329 in R19 at 16%, followed by R07 (10%). Moreover, Type II accounted for more than 5% in seven  
 330 regions: R11, R13, R17, R18, R16, R01, and R06.



331

332 **Figure 5.** Statistical chart of random evaluation results. The ring in the pie chart represents the  
 333 proportion of each type with total number of samples in the region. Pie chart represents the correct  
 334 rate, which is the proportion of the number of Types I and II with region sample quantity. The size  
 335 of the pie/ring represents the grade of the correct rate in the region. Types I, II, and III (See Section  
 336 3.2.4) represent the centerline of correct, inaccurate, and incorrect, respectively.

337

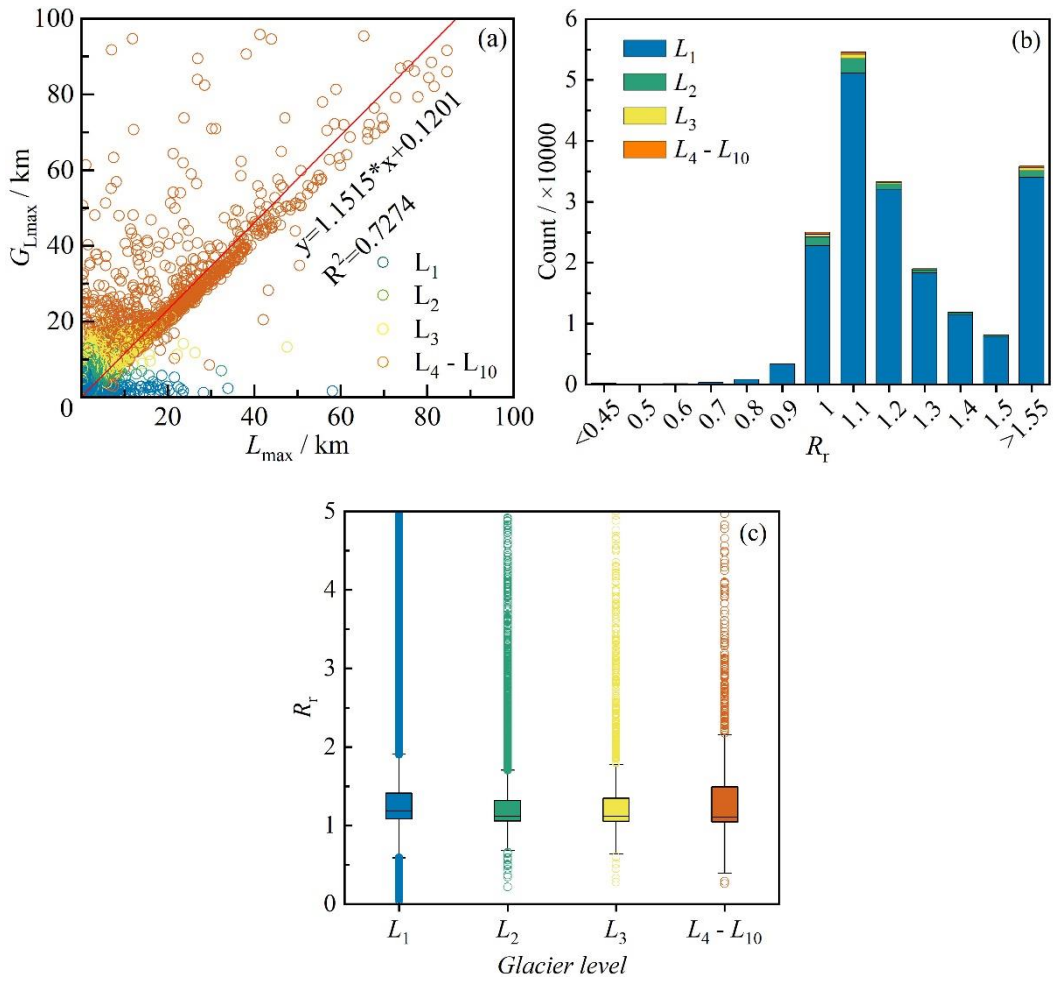
338 The above results indicate that, in addition to the three glacier regions of R07, R09, and R19, the  
 339 random samples of the glacier centerline dataset have excellent performance in terms of accuracy,  
 340 particularly in R02, R12, and R14. The unmarked ice cap and local low-quality DEM were the main  
 341 reasons for the poor quality of the glacier centerline in R07 and R09, respectively. Owing to glacier  
 342 complexes and low altitude differences in low-quality DEMs at the glacier tongue, the quality of  
 343 the glacier centerline obtained in R19 was poor. However, from the viewpoint of dataset coverage,  
 344 we provided the extraction results of the glacier centerline in R19.

345

#### 346 4.2.2 Compare with previous results

347 After applying this algorithm to the global glacier inventory RGI v6.0, we compared the glacier  
 348 lengths ( $G_{Lmax}$ ) automatically obtained in this study with those ( $L_{max}$ ) obtained by Machguth and  
 349 Huss (2014) (Fig. 6). After eliminating 5408 glaciers with  $L_{max}$  value of -9 (no results), the length  
 350 values of the other 192728 glaciers in the global glacier length dataset were directly compared. The  
 351  $G_{Lmax}$  and  $L_{max}$  were generally comparable (Fig. 6a). The glaciers in grades  $L_4-L_{10}$  showed excellent  
 352 fitting degrees, while those of  $L_1-L_3$  determined the linear correlation coefficient owing to their  
 353 large number. The number of glaciers with a length ratio ( $R_l$ ) between  $G_{Lmax}$  and  $L_{max}$  greater than

354 1.55 (Fig. 6b) was approximately 35,000, which were excluded from histogram statistics because  
 355 there was a high probability that the length of at least one of the two datasets was erroneous. The  
 356 peak value of the histogram (Fig. 6b) of  $R_r$  is in the interval 1.05–1.15 and  $R_r$  in the interval 0.95–  
 357 1.25 accounts for 64.55%. The glacier length  $G_{L_{\max}}$  in this study was generally longer than  $L_{\max}$  and  
 358 the average value was approximately 10%, which indicates that glacier centerline lengths were  
 359 probably underestimated in previous studies. In addition, the abnormal value of the length ratio of  
 360 glacier  $L_1$  was the highest and the median value was high (Fig. 6c). The  $R_r$  values of glaciers  $L_4$ – $L_{10}$   
 361 fluctuated greatly. The  $R_r$  distributions of glaciers  $L_2$  and  $L_3$  were relatively concentrated. The reason  
 362 for this is that the length of glacier  $L_1$  was affected by the DEM, while glaciers  $L_4$ – $L_{10}$  were mainly  
 363 disturbed by differences in glacier scale and the accuracy of the auxiliary line.



364

365

366 **Figure 6.** Comparison of longest centerlines calculated in this study and by Machguth and Huss  
 367 (2014). (a) Linear regression of maximum length for all input glaciers (*IGODS*), determined in the  
 368  $G_{L_{\max}}$ , calculated in this study and  $L_{\max}$  obtained in Machguth and Huss (2014). (b) Histogram of  
 369 length ratio ( $R_r$ ,  $G_{L_{\max}}/L_{\max}$ ) for distinct grades of glaciers. (c) Box plots of length ratio ( $R_r$ ) for  
 370 different scales of glaciers.

371

372 Comparisons between  $G_{L_{\max}}$  and  $L_{\max}$  for each first-order glacier region and all random samples are  
 373 shown in Appendix B. There was a preferable fitting degree between  $G_{L_{\max}}$  and  $L_{\max}$  in seven glacier  
 374 regions including R01, R04, R07, and R12–R15, in which the  $R^2$  was larger than 0.95 (Fig. B1).  
 375 The  $R_r$  in R17 ( $R^2 = 0.8174$ ), R05 ( $R^2 = 0.8136$ ), and R03 ( $R^2 = 0.6311$ ) were poor, whereas that in

376 R19 ( $R^2 = 0.5487$ ) was the worst. The  $R^2$  values of the other eight glacier regions were between 0.85  
377 and 0.95. The histograms (Fig. B2) suggest that  $G_{L_{max}}$  and  $L_{max}$  fitted well in R04, R06, R07, R09,  
378 and R12–R15 because they had recognizable single peak values. The peak values of R03, R05, R17,  
379 and R19 were not prominent and the proportion of glaciers with  $R_r > 1.55$  was extremely high,  
380 further increasing the uncertainty in glacier length results in these four regions. R01, R07, R08,  
381 R11–R15, and R18 performed well in the box plot (Fig. B3), whereas the results for R09 were not  
382 good. Moreover, the fitting degree of all random samples was poor (Fig. B1,  $R^2 = 0.7547$ ), the peak  
383 value was more prominent (Fig. B2), and the length ratio distribution of glaciers of different grades  
384 was relatively scattered (Fig. B3). In general, the glacier lengths of R07 and R12–R15 were the  
385 closest, while there were significant differences in R03, R05, R17, and R19.

386  
387 Furthermore, graphic results collected for the maximum length of glaciers in parts of High Asia  
388 (Machguth and Huss, 2014) were used to compare the results. In two parts of R15, Mount  
389 Qomolangma and its surrounding area (Fig. 7a) and Kangchenjunga and its surrounding area (Fig.  
390 7b), the glaciers showed a flaky distribution for mapping. Visible comparison was suggested that  
391 the extraction method used in this study had likely a strong ability to obtain the maximum length of  
392 glaciers (Fig. 7a) and that its sensitivity to topography was lower than that of Machguth and Huss  
393 (2014) (Fig. 7b). Both sets of glacier length extraction schemes were valid and there were large  
394 differences only in a few glaciers or in certain types of glaciers, such as slope glaciers and ice caps.

395

#### 396 **4.2.3 Uncertainties and possibilities for improvement**

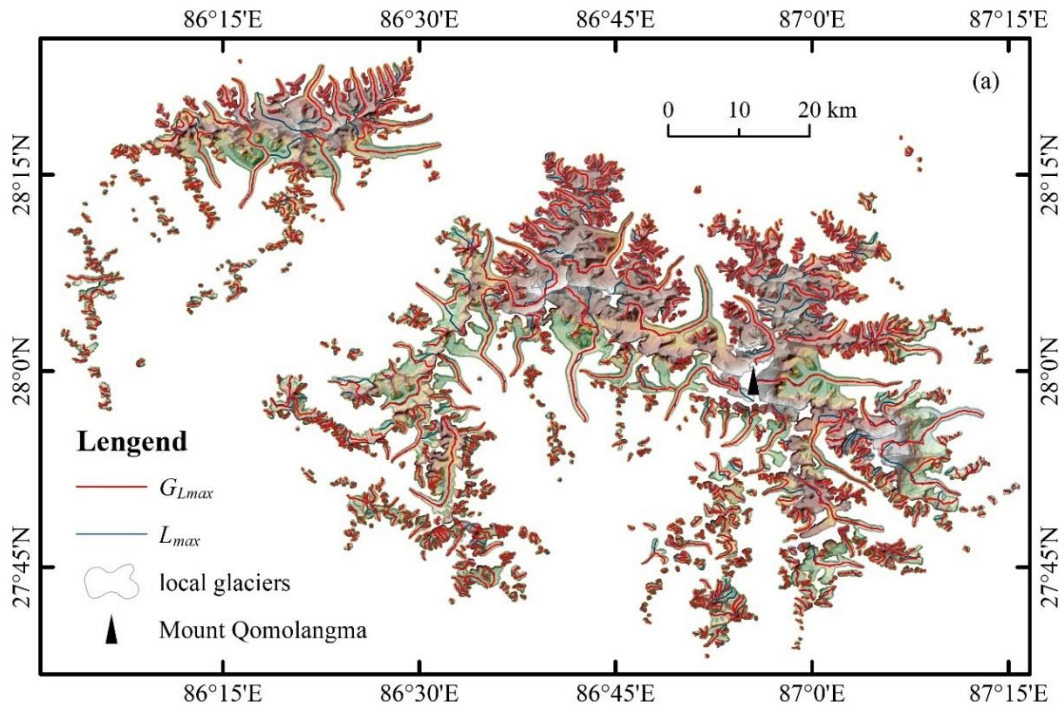
397 Although we compared the two current global length datasets, it is still difficult to accurately reflect  
398 the quality of the dataset in this study. For some glaciers that are not provided centerlines in this  
399 dataset, data users need to update the corresponding glacier outlines and could use the automatic  
400 extraction tool provided in this study to generate their centerlines, which involves the defective  
401 glacier outlines (*FGODS*), nominal glaciers and ice caps of the RGI v6.0. Specifically, the  
402 centerlines of the *FGODS* rely on the glacier outlines that meet the requirements of this study. These  
403 glacier outlines include glacier inventory data from other sources, or the *FGODS* that are repaired  
404 by some algorithms or manual process. Nominal glaciers are similar to *FGODS*, and also require  
405 users to obtain corresponding glacier outlines. Automatic approaches dividing ice caps from glacial  
406 complexes into individual glaciers are currently limited, and data users can only use their own  
407 criterion to divide ice caps and then use our tool to generate centerlines. In addition, prioritizing the  
408 coverage of this dataset, we designed a geometry-based algorithm to repair *FGODS* and provided  
409 data users with their centerlines in the form of supplementary dataset, and corresponding codes and  
410 results can be seen in sub-datasets *CODES* and *SUP\_220707*.

411

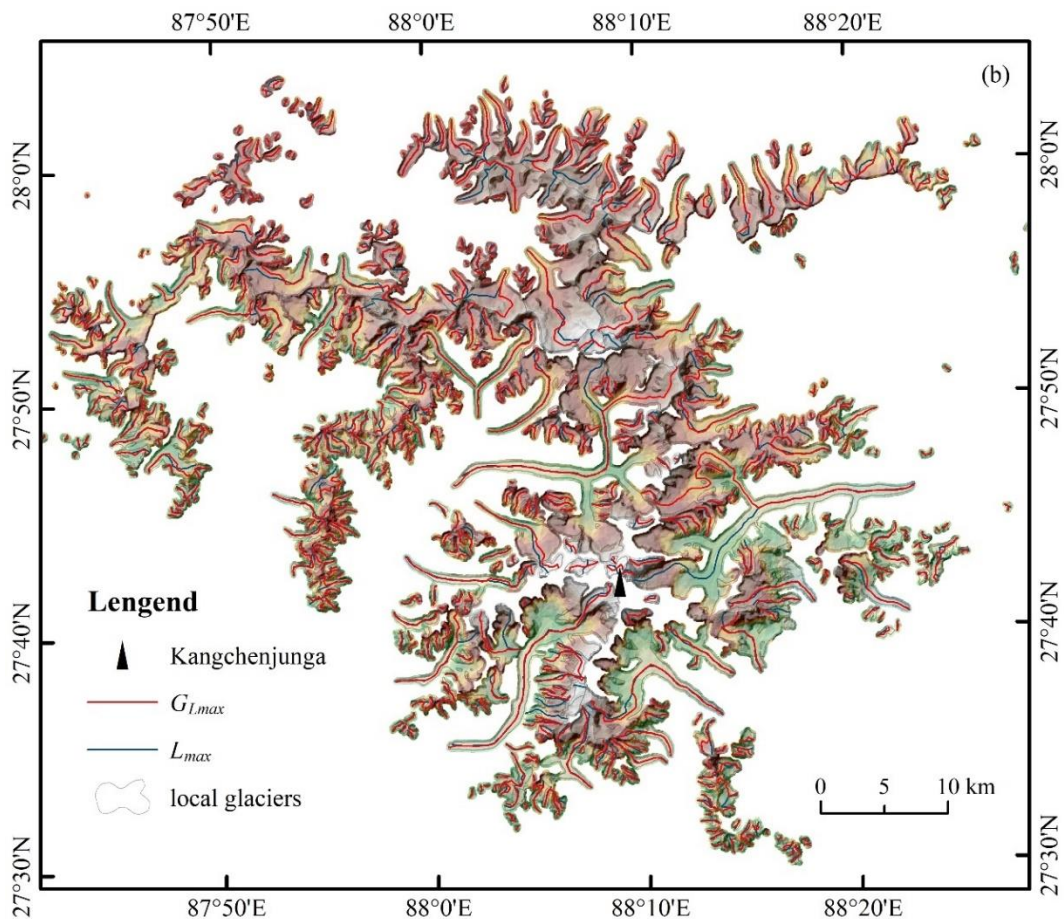
412 The automatic extraction algorithm in this study is more suitable for application to single-outlet  
413 glaciers, particularly valley glaciers; it is not suitable for ice caps, flat-top glaciers, and tidal glaciers  
414 that are widely distributed in the Antarctic, sub-Antarctic, northern Canadian Arctic, and other areas.  
415 In short, the uncertainties in this dataset come probably from the centerlines of some slope glaciers  
416 and the ice caps that are not identified in RGI v6.0, or a few centerlines with unpredictable quality  
417 due to the input data such as the incorrect glacier polygons, erroneous DEMs. In future work, better  
418 glacier inventory and more accurate DEM are useful for the improvement of centerline quality. On  
419 the other hand, optimizing the automatic glacier segmentation approach, DEM-based extraction

420 algorithm of glacier feature lines and centerline trade-off algorithm are also probable ways to further  
421 improve the accuracy of glacier centerlines. In addition, it is probably beneficial to further clarify  
422 the type of each glacier in the glacier inventory for the estimates of centerline accuracy.  
423





424



425

426 **Figure 7.** Visible comparison of the longest center lines calculated in this study and by Machguth  
 427 and Huss (2014). The figure shows two glacier-covered regions in the Himalayas, covering Mount  
 428 Qomolangma (**panel a**) and Kangchenjunga (**panel b**, the world's third highest mountain) and their  
 429 surrounding areas. The background is the DEM used for the calculation.



430 **5 Data availability**

431 Global glacier centerline dataset (*GGCLDS*), global glacier maximum length dataset (*GGMLDS*),  
 432 and other relevant datasets are available at <https://doi.org/10.11922/sciencedb.01643> (Zhang and  
 433 Zhang, 2022). All 17 sub-datasets of this dataset are listed in Table 5.

434 **Table 5.** Description of the members contained in this dataset.

Acronym	Data format	Data volume	Description
<i>IGODS</i>	*.shp	316 MB	Input glacier outline dataset
<i>GGEDS</i>	*.tif	3.70 GB	Global glacier elevation dataset
<i>GGCLDS</i>		838 MB	Global glacier centerline dataset
<i>GGMLDS</i>		616 MB	Global glacier maximum length dataset
<i>GACLDS</i>		302 MB	Global glacier accumulation region length dataset
<i>GABLDS</i>		358 MB	Global glacier ablation region length dataset
<i>GOSRDS</i>		1.16 GB	Global glacier outline segmentation result dataset
<i>GLHPDS</i>		11 MB	Global glacial local highest point dataset
<i>GLPDS</i>	*.shp	6.25 MB	Global glacial lowest point dataset
<i>GUGODS</i>		3.95 MB	Unsuccessful global glacier outline dataset
<i>FGODS</i>		119 MB	Global flawed glacier outline dataset
<i>GGECDs</i>		334 MB	Global glacier external contour dataset
<i>GGBMDS</i>		374 MB	Global glacier buffer mask dataset
<i>MHMLDS</i>		8.32 MB	The maximum length of Machguth and Huss in High Asia
<i>SUP_220707</i>		681 MB	Updated the centerlines of the repaired <i>FGODS</i>
<i>CODES</i>	*.py	40 KB	Related codes of data process in bulk
<i>LOGS</i>	*.txt	1.27 MB	Related logfiles of data process in bulk

435

436 **6 Conclusions**

437 In this study, a new dataset on the centerline of global glaciers was constructed and the maximum  
 438 length was calculated based on the global glacier inventory (RGI v6.0) and global glacier region  
 439 DEM (*GGEDS*, composed of NASADEM, ASTER GDEM v3, and Copernicus DEM). In total,  
 440 198,137 glacier centerlines were generated, accounting for 99.74% of the total number of imported  
 441 glaciers (*IGODS*) and 91.52% of the total number of the global glacier inventory. The  
 442 comprehensive extraction accuracy of these glacier centerlines (*GGCLDS*) used in random self-  
 443 assessment was 89.68%. The glacier length ( $G_{L_{max}}$ ) obtained in this study was generally  
 444 approximately 10% longer than that of  $L_{max}$  on average. Nevertheless, our method showed a stronger  
 445 ability to obtain the maximum length, and we believe that the resulting errors were controllable.  
 446 Furthermore, the preprocessing algorithm we designed accurately identified 10,764 erroneous  
 447 glacier polygons from RGI v6.0, which formed the defective glacier dataset (*FGODS*).

448

449 A dataset containing 17 sub-datasets was generated through the above work, including two basic  
 450 input datasets (*IGODS* and *GGEDS*), two key result datasets (*GGCLDS* and *GGMLDS*), four  
 451 process datasets, six derived result datasets, and three supplementary datasets. Ice caps, nominal  
 452 glaciers, and erroneous glacier polygons were eliminated from most sub-datasets in this study,  
 453 accounting for approximately 8.25% of the total RGI v6.0. The poor status of these glacier polygons  
 454 was not sufficient to support the automatic extraction of glacier centerlines, which needs to be  
 455 improved in future work. Inevitably, there were some defects in the algorithm or datasets that need  
 456 to be considered in future research. For instance, the glacial regions (R19 and R03) with the worst  
 457 results were added to the dataset to prioritize data coverage integrity. It is worth noting that the  
 458 global glacier DEM dataset (*GGEDS*), global glacier external outline dataset (*GGECDs*), and global  
 459 glacier buffer mask datasets (*GGBMDS*) cover all glaciers in RGI v6.0. Accordingly, they will help

460 researchers design more efficient automated extraction algorithms to produce datasets containing  
 461 all types of glacier centerlines and lengths worldwide, which is our next goal.

462

463 **Appendix A:** Model parameters resulting from the Central Asia Glacier and extended to worldwide  
 464 calculations are listed in Table A1.

465 **Table A1.** Parameterization scheme for extracting global glacier centerlines.

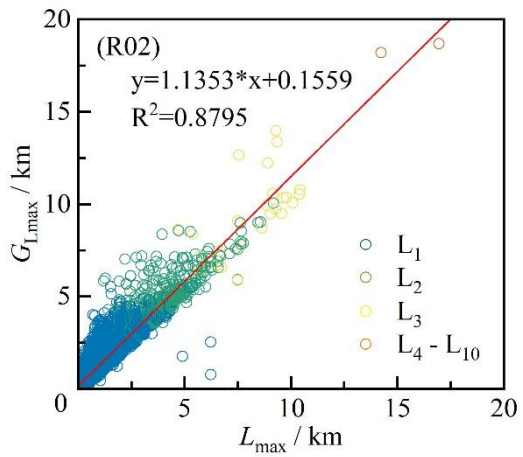
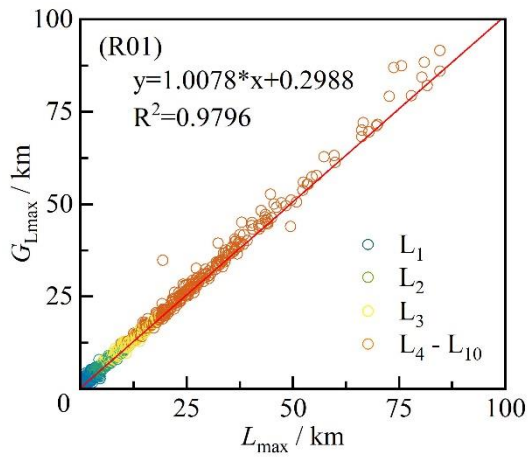
Par.	Description	Value (Levels 1-10)	Unit
$P_1$	Maximum distance between adjacent vertexes	10	m
$P_2$	Buffer distance outside the glacier outline	30	m
$P_3$	Threshold of accumulative flow	5 - 8, 10, 20, 30, 50, 100, 200	int $\times 10^3$
$P_4$	Length of the shortest auxiliary line	10 - 19	int
$P_5$	Length of the longest auxiliary line	2 - 11	int
$P_6$	Interval for searching the local highest points	50, 60, 70, 80, 90, 100, 200, 300, 400, 500	count
$P_7$	Matching tolerance of the vertexes of polyline	0.2, 0.2, 0.5, 0.5, 1 ( $L_5 - L_{10}$ )	m
$P_8$	Size of grid cell in Euclidean allocation	1, 5, 15, 15, 30 ( $L_5 - L_{10}$ )	m
$P_9$	Minimum distance between the adjacent $P_{\max}$	10, 15, 30, 60, 120, 150, 200, 300, 400, 500	count
$P_{10}$	Smoothing tolerance of polylines	5, 10, 15, 20, 30 ( $L_5 - L_{10}$ )	m
$P_{11}$	Length threshold of the longest auxiliary line	10190	km <sup>2</sup>

466 **Notes:** The calculation method for each parameter is detailed in Zhang et al. (2021).  $P_{\max}$  and  $L$  refer to the local  
 467 highest points and grades of the glacier, respectively.

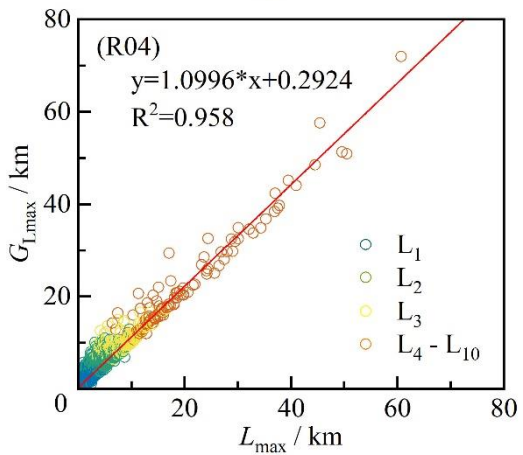
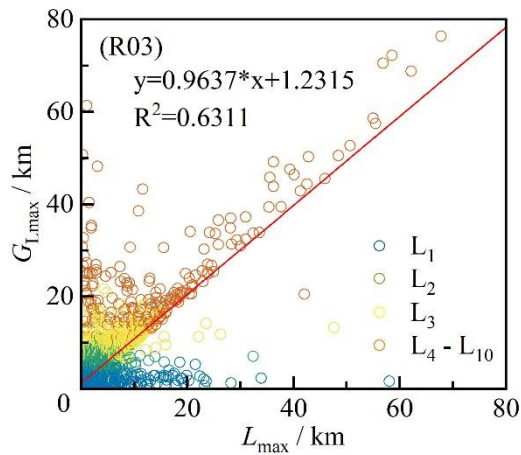
468

469 **Appendix B:** Comparison of longest centerlines calculated in this study and by Machguth and Huss  
 470 (2014) for all samples and the different first-order glacier regions of RGI v6.0. Linear regression of  
 471 the two lengths, histogram of length ratio ( $R_r$ ), and box plots of  $R_r$  for glaciers of different grades in  
 472 these regions were in Figure B1, B2, and B3, respectively.

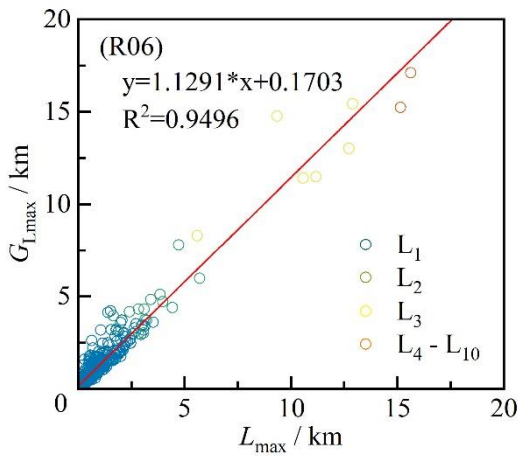
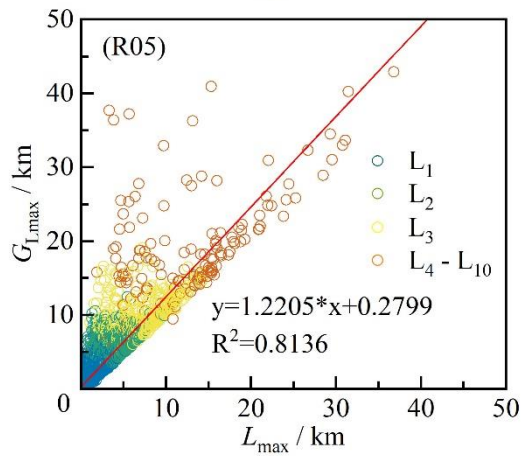
473



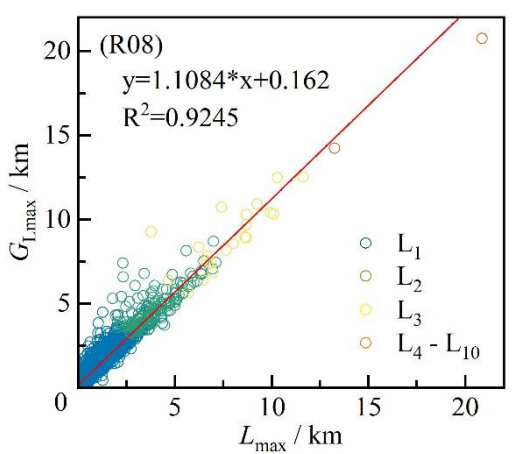
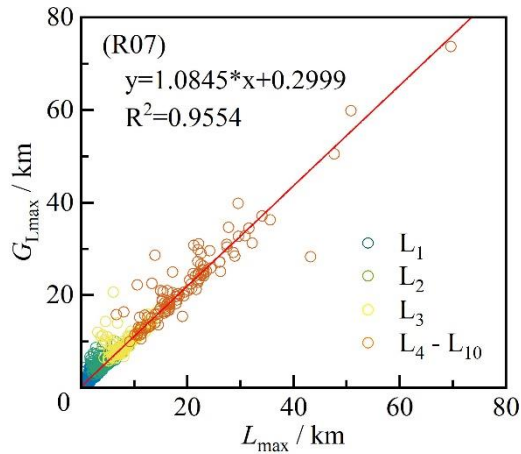
474



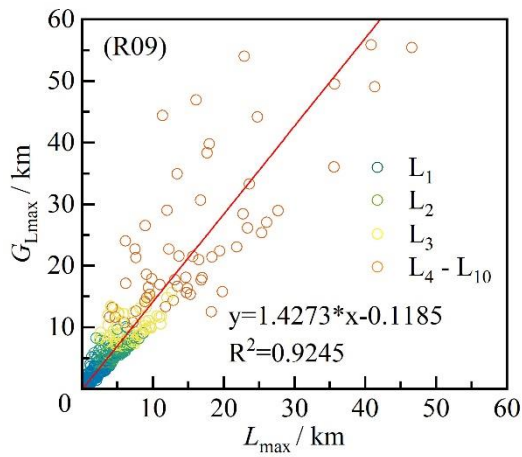
475



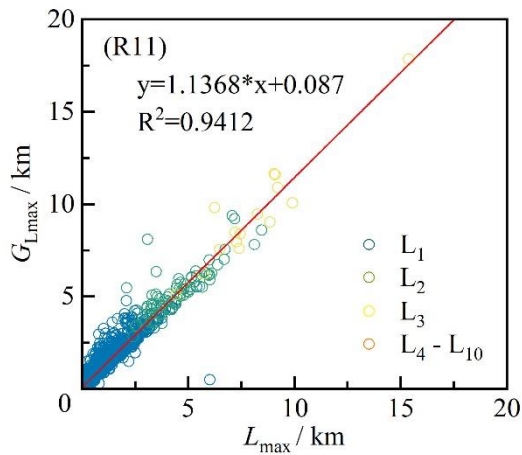
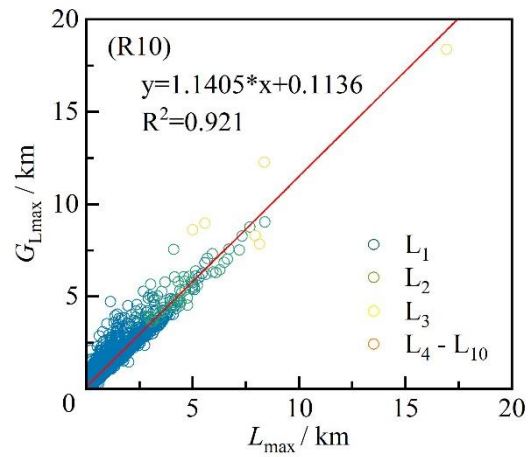
476



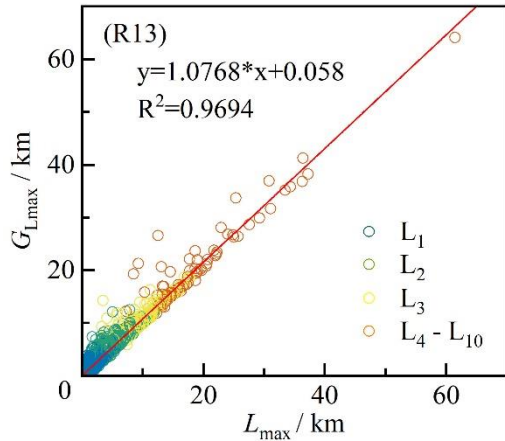
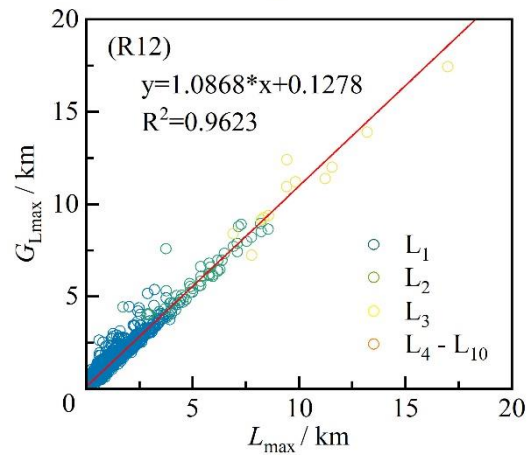
477



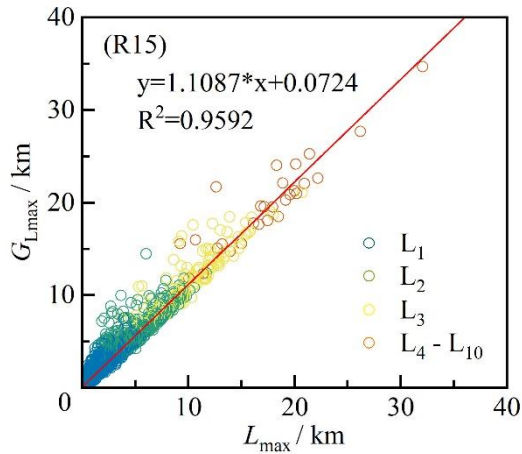
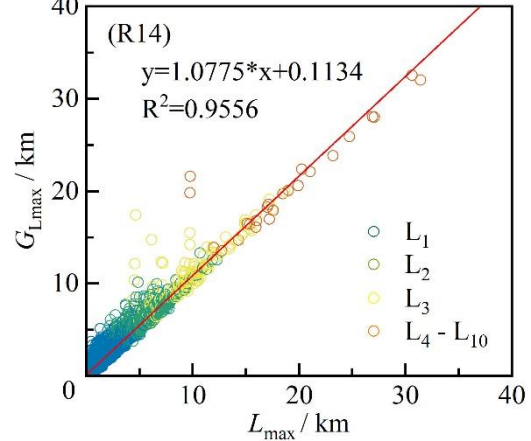
478



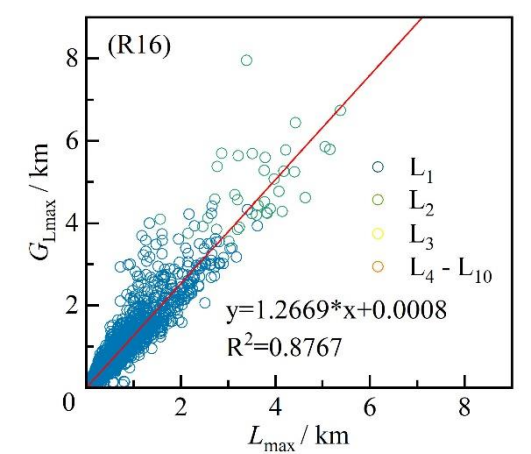
479

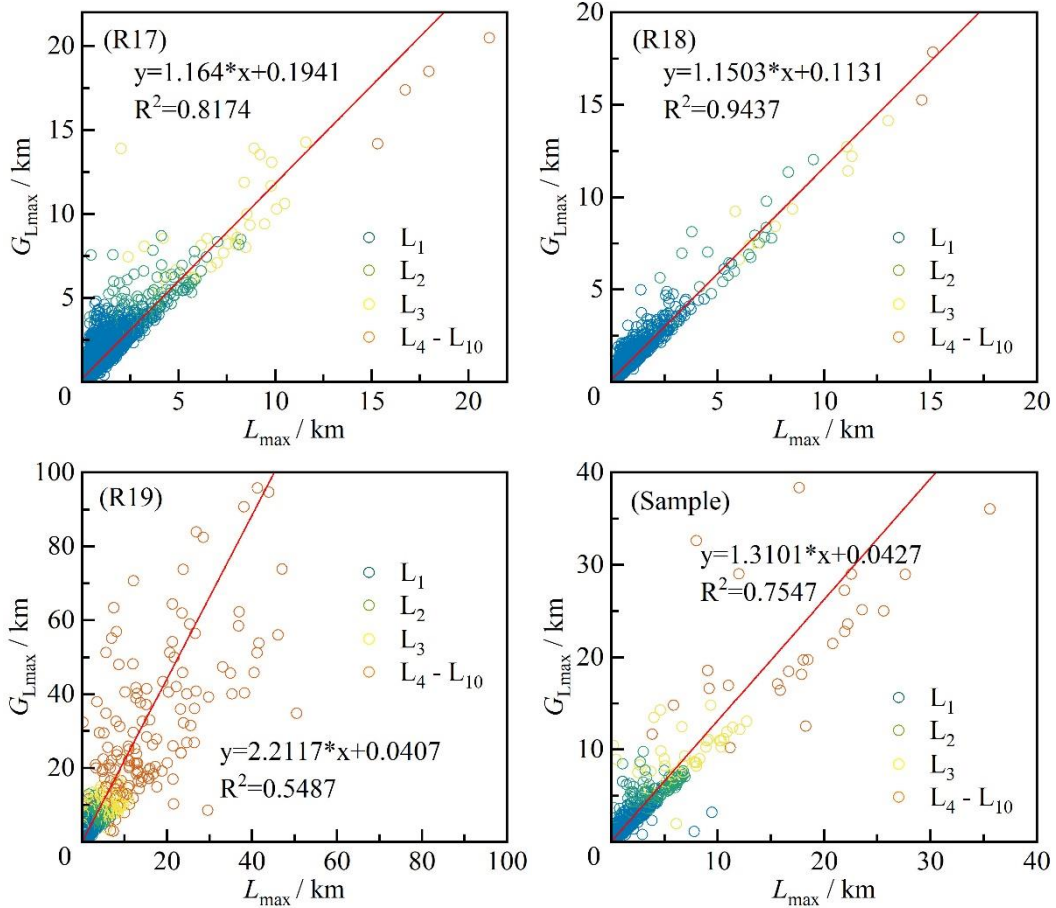


480



481





482

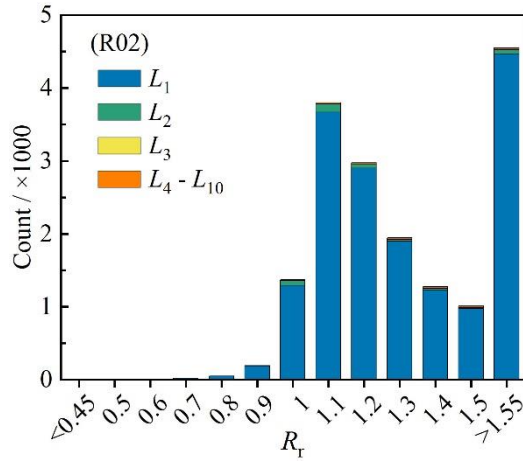
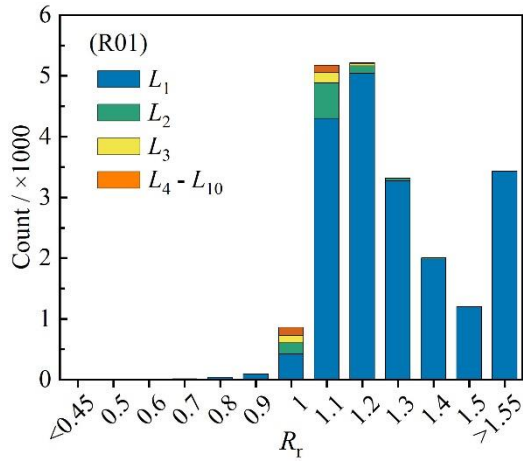
483

484

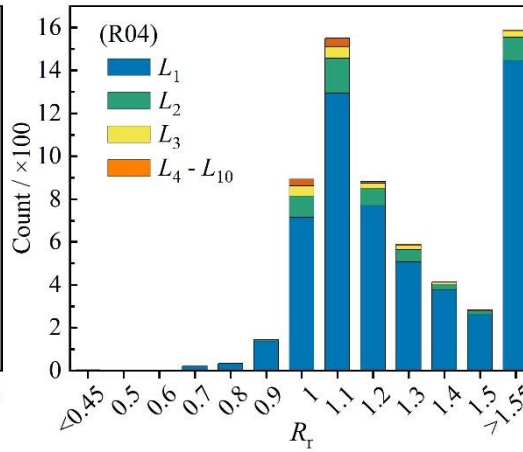
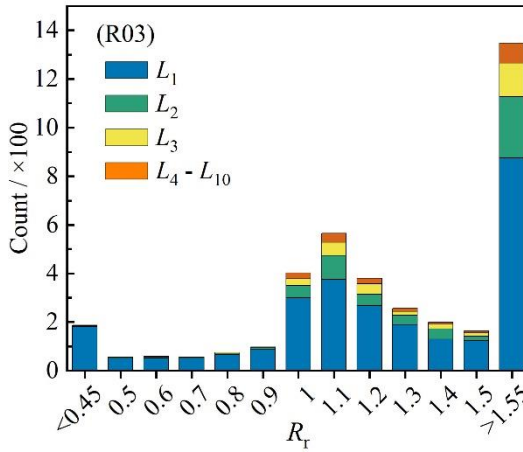
**Figure B1.** Linear regression in different glacier regions between glacier length ( $G_{L_{max}}$ ) calculated in this study and glacier length ( $L_{max}$ ) calculated by Machguth and Huss (2014).

485

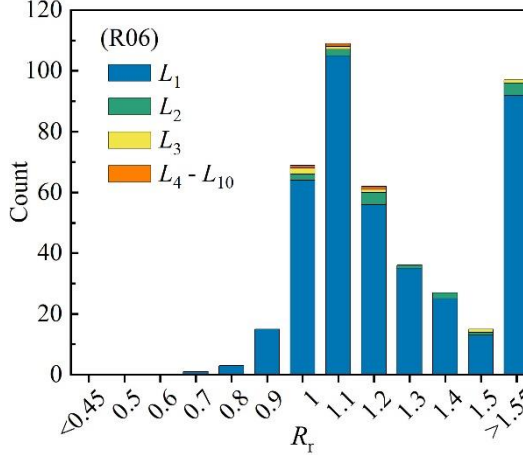
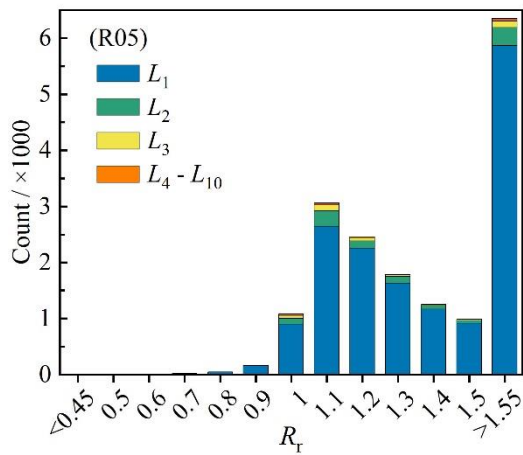
486



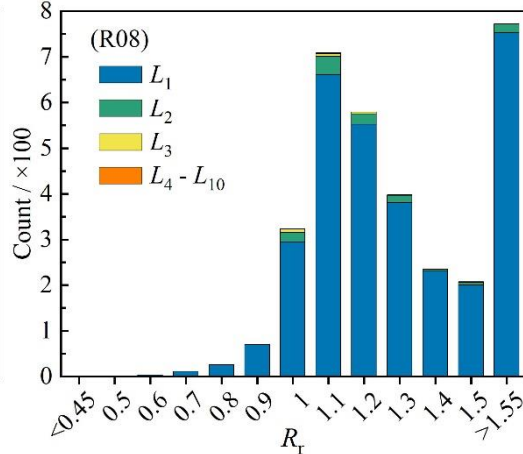
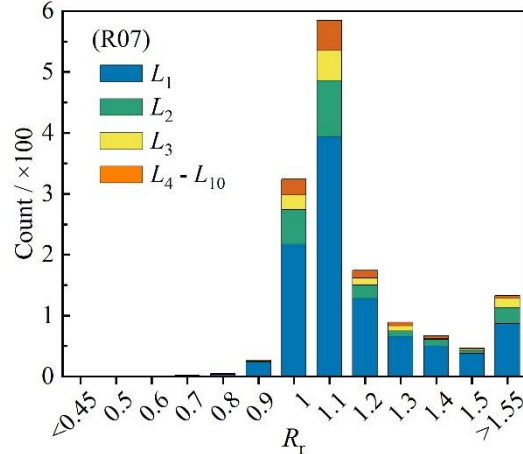
487



488

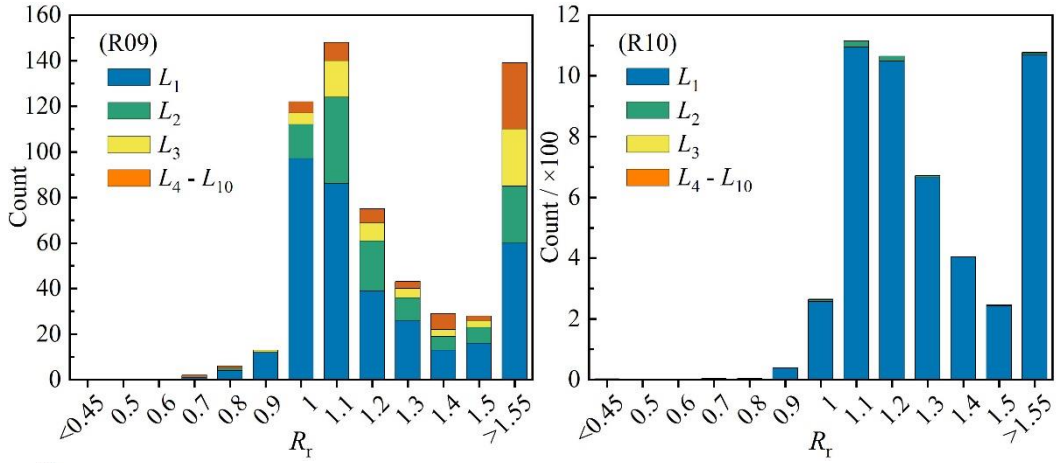


489

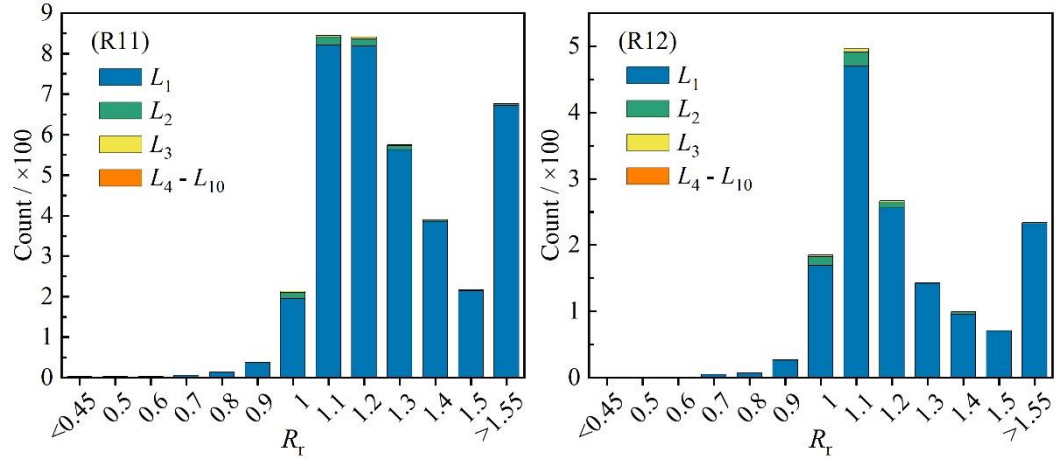


490

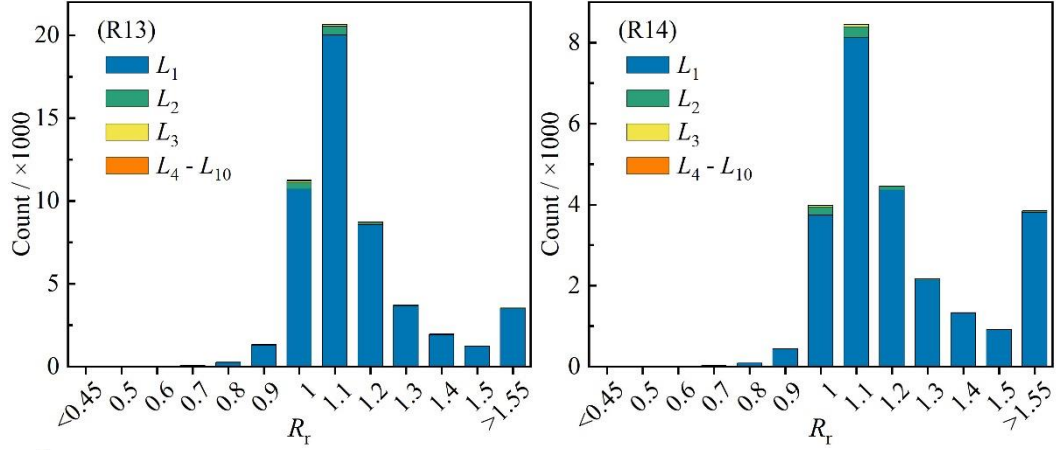




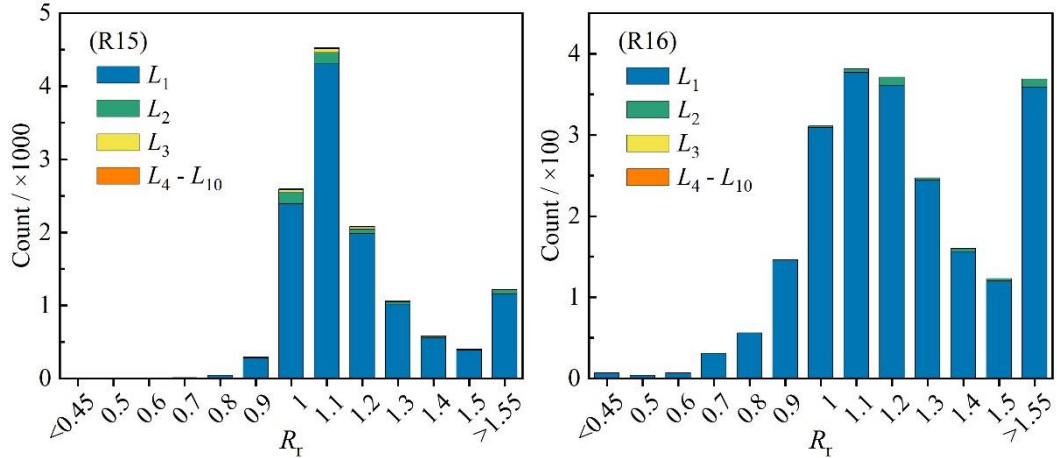
491



492

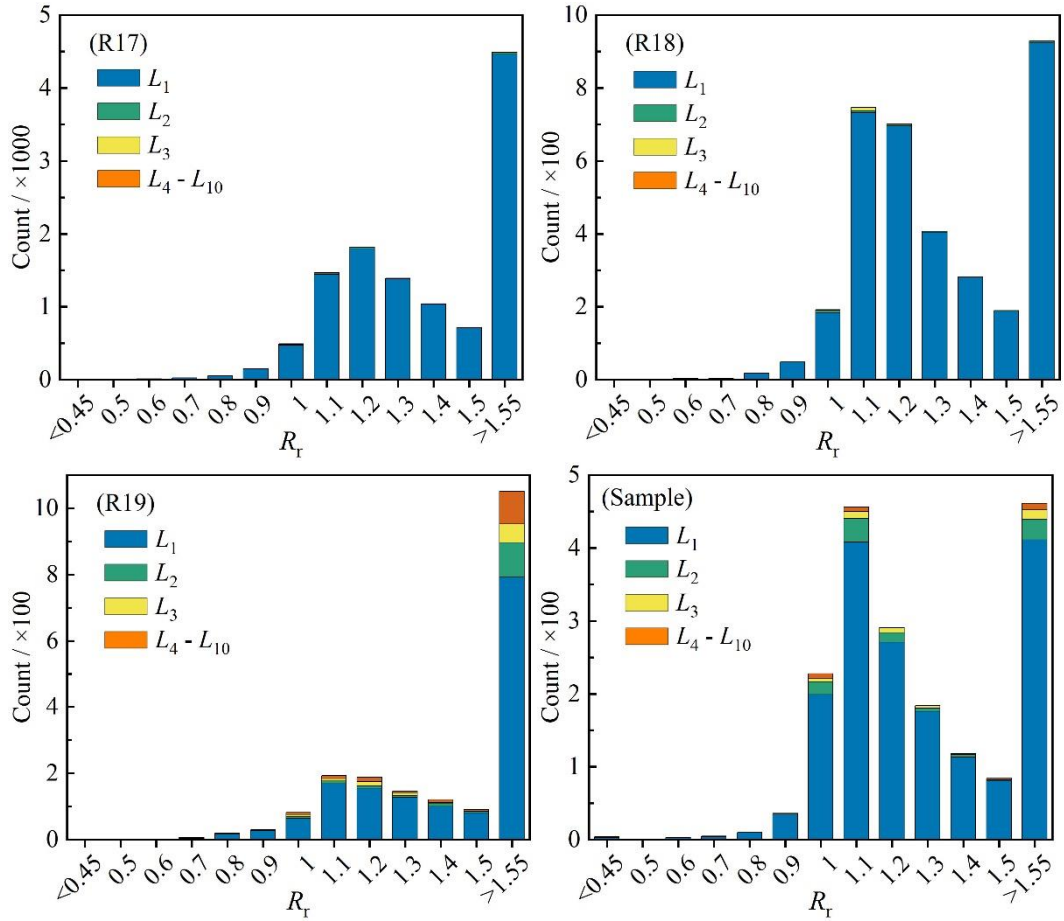


493



494





495

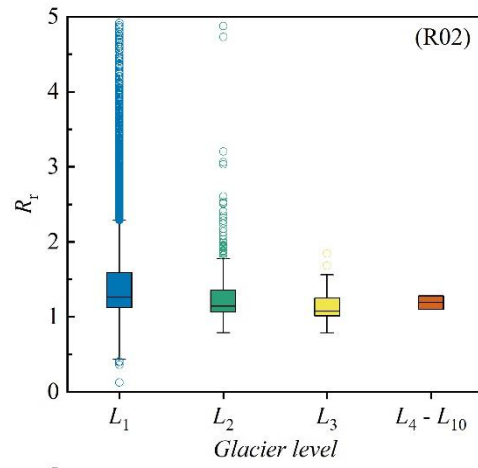
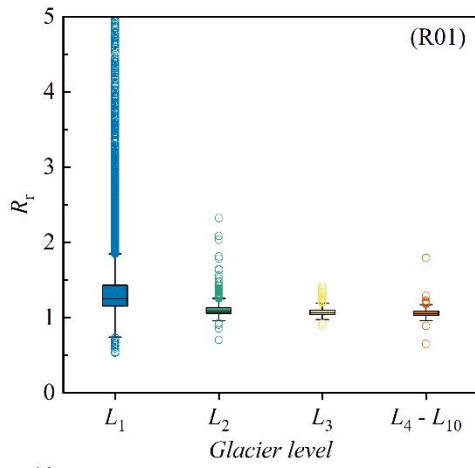
496

497

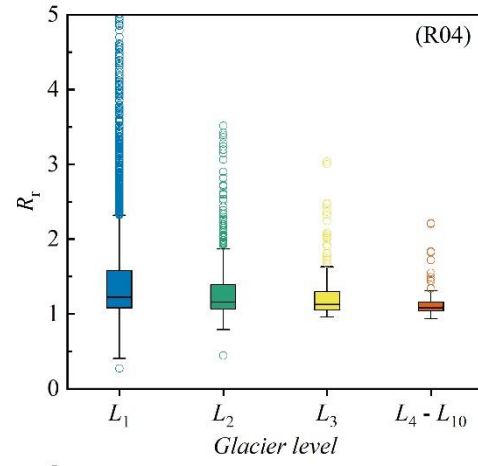
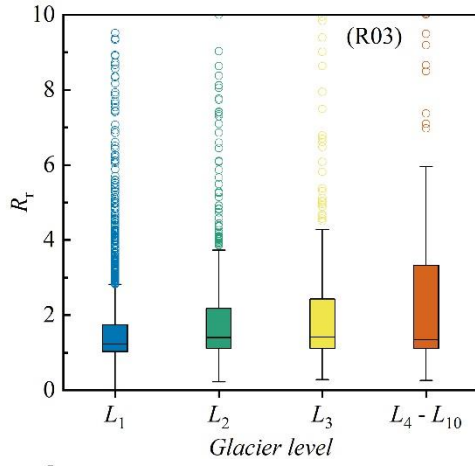
**Figure B2.** Histograms of the length ratio ( $R_r$ ,  $G_{L_{\max}}/L_{\max}$ ) of distinct glacier grades in glacier-covered regions and all samples.

498

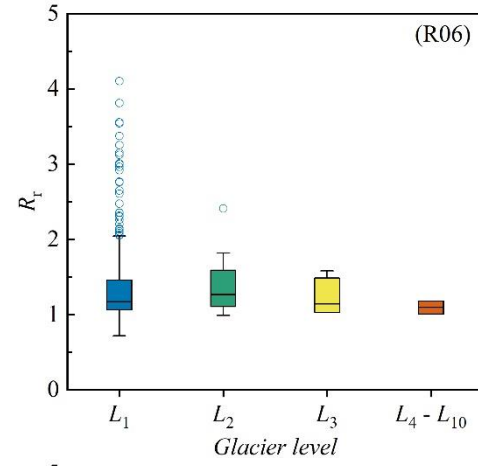
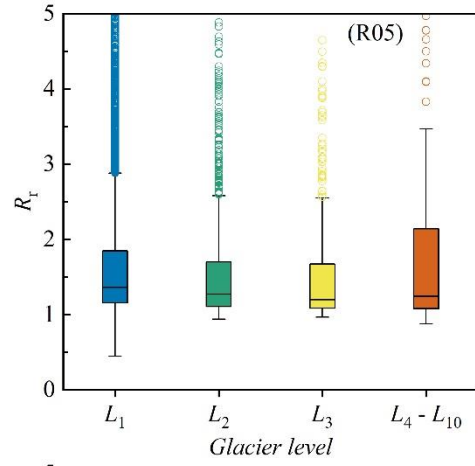
499



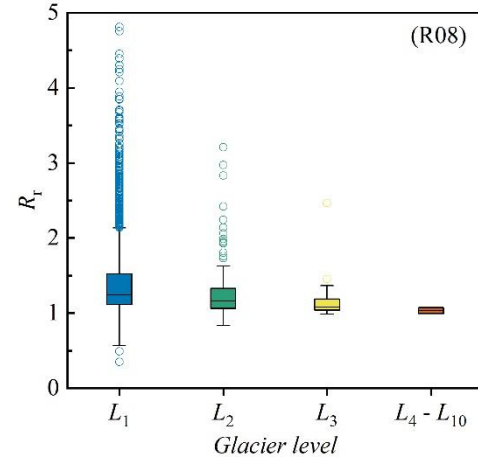
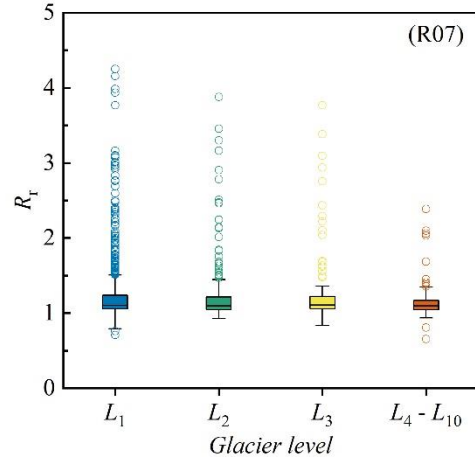
500



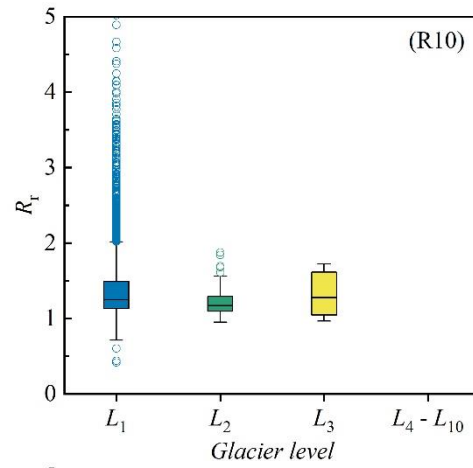
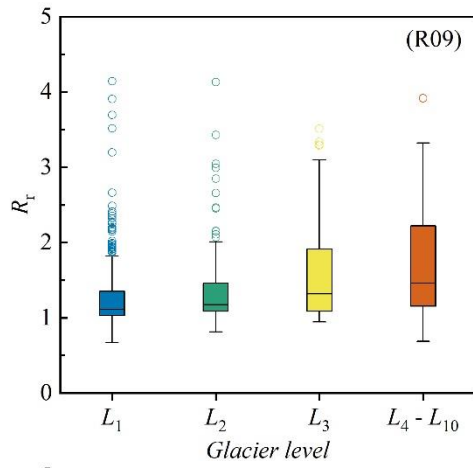
501



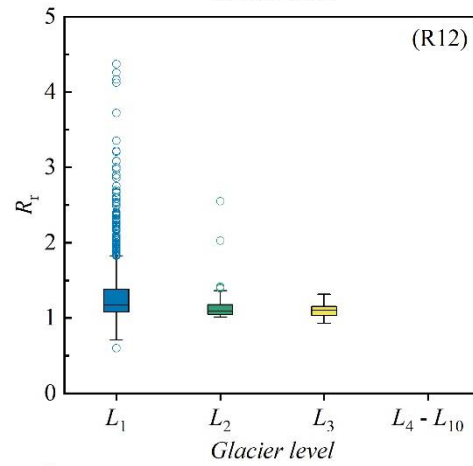
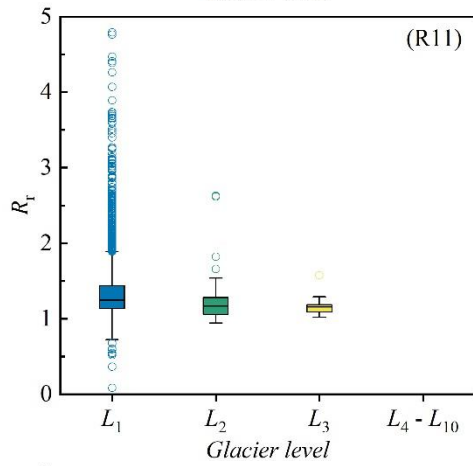
502



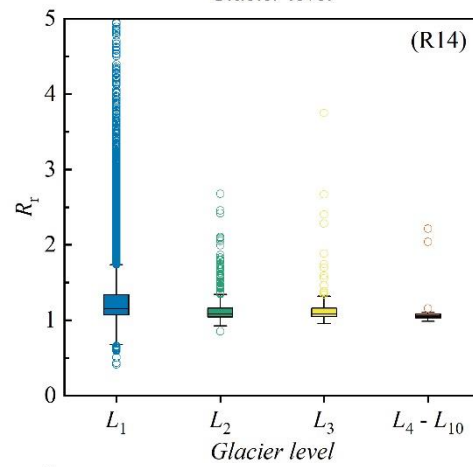
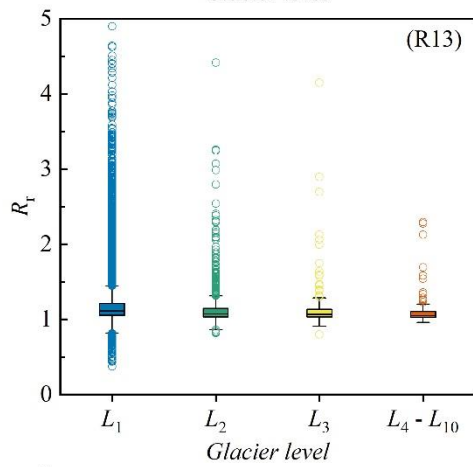
503



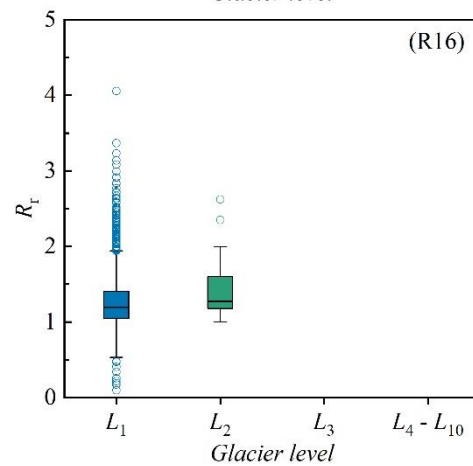
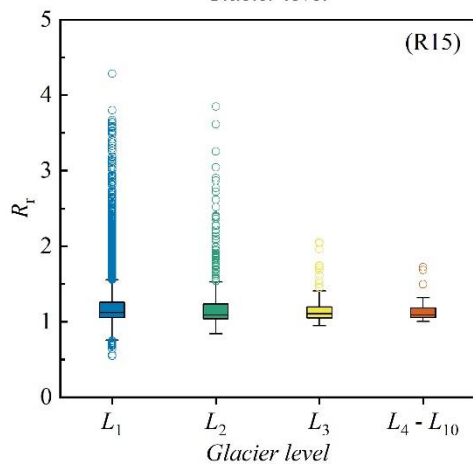
504



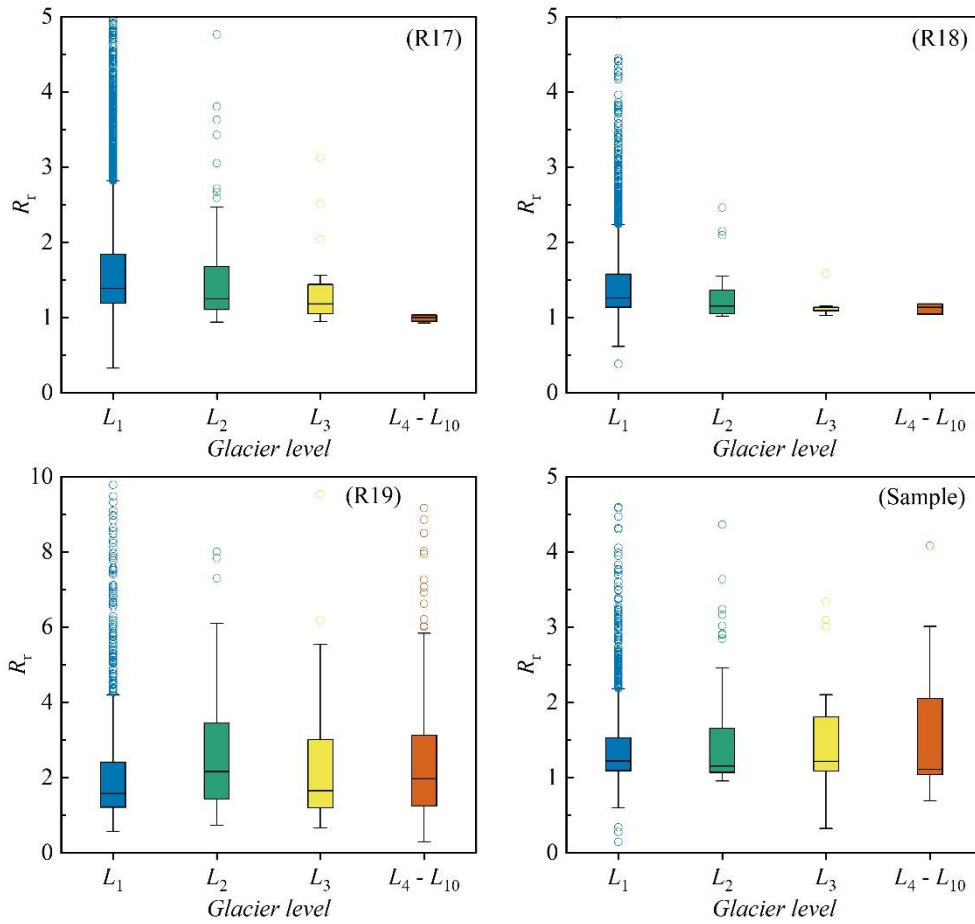
505



506



507



508

509

510

511

512

**Figure B3.** Box plots of length ratio ( $R_r$ ,  $G_{L_{\max}}/L_{\max}$ ) of glaciers of distinct grades in every glacier-covered region and whole sample.

513 **Supplement.**

514 The Supplement consists of two parts: (1) ‘GlacierCenterlines\_Py27’ (version 5.2.1), the updated  
515 automatic extraction tool of glacier centerlines in this study, which fixed some defects compared  
516 with version 5.2.0 (<https://doi.org/10.5194/tc-151955-2021-supplement>). (2)  
517 ‘Other\_parameters\_T1.txt’ is the parameter file for extracting the global glacier centerlines.

518

519 **Author contributions.**

520 All authors contributed to writing and editing the manuscript. DZ processed the data, performed all  
521 calculations, created all figures, and wrote most of the manuscript. SZ contributed significantly to  
522 the development of the analyses, figures, and writing. XY contributed to the development of the  
523 data production strategy and writing. GZ and WL contributed to the initial data production. SW  
524 participated in writing Chapter 4.

525

526 **Competing interests.**

527 The authors declare that they have no conflict of interest.

528

529 **Acknowledgments.**

530 We thank editors, two reviewers and community scholars for their valuable comments that improved  
531 the manuscript. The authors would especially like to thank GLIMS for releasing the RGI v6.0  
532 (<http://www.glims.org/RGI/andolph.html>, last accessed: November 15, 2021), LP DAAC for  
533 releasing the NASADEM (<https://lpdaac.usgs.gov/news/release-nasadem-data-products/>, last  
534 accessed: November 17, 2021), METI and NASA for jointly releasing the ASTER GDEM v3  
535 (<https://lpdaac.usgs.gov/news/nasa-and-meti-release-aster-global-dem-version-3/>, last accessed:  
536 November 17, 2021), and the European Space Agency (ESA) for providing the Copernicus DEM  
537 (<https://spacedata.copernicus.eu/web/cscda/cop-dem-faq>, last accessed: November 17, 2021). This  
538 work is not possible without the support of open-access data.

539

540 **Financial support.**

541 This research was funded by the Second Tibetan Plateau Scientific Expedition and Research  
542 Program (STEP) (grant number: 2019QZKK020109) and China National Natural Science  
543 Foundation (grant numbers: 41730751, 42171124).

544

545 **References**

546 Abrams, M., Crippen, R., and Fujisada, H.: ASTER Global Digital Elevation Model (GDEM) and  
547 ASTER Global Water Body Dataset (ASTWBD), Remote Sensing, 12,  
548 <https://doi.org/10.3390/rs12071156>, 2020.

549 Aciego, S. M., Stevenson, E. I., and Arendt, C. A.: Climate versus geological controls on glacial  
550 meltwater micronutrient production in southern Greenland, Earth and Planetary Science Letters,  
551 424, 51-58, <https://doi.org/10.1016/j.epsl.2015.05.017>, 2015.

552 Carabajal, C. C. and Boy, J. P.: Evaluation of Aster Gdem V3 Using Icesat Laser Altimetry, ISPRS -  
553 International Archives of the Photogrammetry, Remote Sensing and Spatial Information Sciences,  
554 XLI-B4, 117-124, <https://doi.org/10.5194/isprsarchives-XLI-B4-117-2016>, 2016.

555 Carrera-Hernández, J. J.: Not all DEMs are equal: An evaluation of six globally available 30 m resolution  
556 DEMs with geodetic benchmarks and LiDAR in Mexico, Remote Sensing of Environment, 261,

557 <https://doi.org/10.1016/j.rse.2021.112474>, 2021.

558 Cazenave, A.: Global sea-level budget 1993–present, *Earth System Science Data*, 10, 1551-1590,  
559 <https://doi.org/10.5194/essd-10-1551-2018>, 2018.

560 Farinotti, D., Huss, M., Fürst, J. J., Landmann, J., Machguth, H., Maussion, F., and Pandit, A.: A  
561 consensus estimate for the ice thickness distribution of all glaciers on Earth, *Nature Geoscience*, 12,  
562 168-173, <https://doi.org/10.1038/s41561-019-0300-3>, 2019.

563 Farr, T. G., Rosen, P. A., Caro, E., Crippen, R., Duren, R., Hensley, S., Kobrick, M., Paller, M., Rodriguez,  
564 E., Roth, L., Seal, D., Shaffer, S., Shimada, J., Umland, J., Werner, M., Oskin, M., Burbank, D., and  
565 Alsdorf, D.: The Shuttle Radar Topography Mission, *Reviews of Geophysics*, 45, 1-33,  
566 <https://doi.org/10.1029/2005rg000183>, 2007.

567 Gao, Y. P., Yao, X. J., Liu, S. Y., Qi, M. M., Gong, P., An, L. N., Li, X. F., and Duan, H. Y.: Methods and  
568 future trend of ice volume calculation of glacier, *Arid Land Geography*, 41, 1204-1213,  
569 <https://doi.org/10.12118/j.issn.1000-6060.2018.06.08>, 2018.

570 Hansen, K., Hasenstab, K., and Schwartzman, A.: Estimating Mountain Glacier Flowlines by Local  
571 Linear Regression Gradient Descent, *IEEE Transactions on Geoscience and Remote Sensing*, 59,  
572 10022-10034, <https://doi.org/10.1109/tgrs.2020.3035513>, 2020.

573 Heid, T. and Käab, A.: Repeat optical satellite images reveal widespread and long term decrease in land-  
574 terminating glacier speeds, *The Cryosphere*, 6, 467-478, <https://doi.org/10.5194/tc-6-467-2012>,  
575 2012.

576 Herla, F., Roe, G. H., and Marzeion, B.: Ensemble statistics of a geometric glacier length model, *Annals  
577 of Glaciology*, 58, 130-135, <https://doi.org/10.1017/aog.2017.15>, 2017.

578 Herreid, S. and Pellicciotti, F.: The state of rock debris covering Earth's glaciers, *Nature Geoscience*, 13,  
579 621-627, <https://doi.org/10.1038/s41561-020-0615-0>, 2020.

580 Howat, I. M., Porter, C., Smith, B. E., Noh, M.-J., and Morin, P.: The Reference Elevation Model of  
581 Antarctica, *The Cryosphere*, 13, 665-674, <https://doi.org/10.5194/tc-13-665-2019>, 2019.

582 Hugonnet, R., McNabb, R., Berthier, E., Menounos, B., Nuth, C., Girod, L., Farinotti, D., Huss, M.,  
583 Dussailant, I., Brun, F., and Kaab, A.: Accelerated global glacier mass loss in the early twenty-first  
584 century, *Nature*, 592, 726-731, <https://doi.org/10.1038/s41586-021-03436-z>, 2021.

585 Immerzeel, W. W., Lutz, A. F., Andrade, M., Bahl, A., Biemans, H., Bolch, T., Hyde, S., Brumby, S.,  
586 Davies, B. J., Elmore, A. C., Emmer, A., Feng, M., Fernández, A., Haritashya, U., Kargel, J. S.,  
587 Koppes, M., Kraaijenbrink, P. D. A., Kulkarni, A. V., Mayewski, P. A., Nepal, S., Pacheco, P., Painter,  
588 T. H., Pellicciotti, F., Rajaram, H., Rupper, S., Sinisalo, A., Shrestha, A. B., Viviroli, D., Wada, Y.,  
589 Xiao, C., Yao, T., and Baillie, J. E. M.: Importance and vulnerability of the world's water towers,  
590 *Nature*, 577, 364-369, <https://doi.org/10.1038/s41586-019-1822-y>, 2019.

591 Ji, Q., Yang, T.-b., He, Y., Qin, Y., Dong, J., and Hu, F.-s.: A simple method to extract glacier length based  
592 on Digital Elevation Model and glacier boundaries for simple basin type glacier, *Journal of  
593 Mountain Science*, 14, 1776-1790, <https://doi.org/10.1007/s11629-016-4243-5>, 2017.

594 Käab, A., Jacquemart, M., Gilbert, A., Leinss, S., Girod, L., Huggel, C., Falaschi, D., Ugalde, F., Petrakov,  
595 D., Chernomorets, S., Dokukin, M., Paul, F., Gascoïn, S., Berthier, E., and Kargel, J. S.: Sudden  
596 large-volume detachments of low-angle mountain glaciers – more frequent than thought?, *The  
597 Cryosphere*, 15, 1751-1785, <https://doi.org/10.5194/tc-15-1751-2021>, 2021.

598 Kienholz, C., Hock, R., and Arendt, A. A.: A new semi-automatic approach for dividing glacier  
599 complexes into individual glaciers, *Journal of Glaciology*, 59, 925-937,  
600 <https://doi.org/10.3189/2013JoG12J138>, 2013.

601 Kienholz, C., Rich, J. L., Arendt, A. A., and Hock, R.: A new method for deriving glacier centerlines  
602 applied to glaciers in Alaska and northwest Canada, *The Cryosphere*, 8, 503-519,  
603 <https://doi.org/10.5194/tc-8-503-2014>, 2014.

604 Le Bris, R. and Paul, F.: An automatic method to create flow lines for determination of glacier length: A  
605 pilot study with Alaskan glaciers, *Computers & Geosciences*, 52, 234-245,  
606 <https://doi.org/10.1016/j.cageo.2012.10.014>, 2013.

607 Le Moine, N. and Gsell, P.-S.: A graph-based approach to glacier flowline extraction: An application to  
608 glaciers in Switzerland, *Computers & Geosciences*, 85, 91-101,  
609 <https://doi.org/10.1016/j.cageo.2015.09.010>, 2015.

610 Leclercq, P. W. and Oerlemans, J.: Global and hemispheric temperature reconstruction from glacier  
611 length fluctuations, *Climate Dynamics*, 38, 1065-1079, <https://doi.org/10.1007/s00382-011-1145-7>,  
612 2011.

613 Leclercq, P. W., Oerlemans, J., Basagic, H. J., Bushueva, I., Cook, A. J., and Le Bris, R.: A data set of  
614 worldwide glacier length fluctuations, *The Cryosphere*, 8, 659-672, [https://doi.org/10.5194/tc-8-](https://doi.org/10.5194/tc-8-659-2014)  
615 [659-2014](https://doi.org/10.5194/tc-8-659-2014), 2014.

616 Li, H., Ng, F., Li, Z., Qin, D., and Cheng, G.: An extended “perfect-plasticity” method for estimating ice  
617 thickness along the flow line of mountain glaciers, *Journal of Geophysical Research: Earth Surface*,  
618 117, n/a-n/a, <https://doi.org/10.1029/2011jf002104>, 2012.

619 Li, X., Ding, Y., Hood, E., Raiswell, R., Han, T., He, X., Kang, S., Wu, Q., Yu, Z., Mika, S., Liu, S., and  
620 Li, Q.: Dissolved Iron Supply from Asian Glaciers: Local Controls and a Regional Perspective,  
621 *Global Biogeochemical Cycles*, 33, 1223-1237, <https://doi.org/10.1029/2018gb006113>, 2019.

622 Li, Y., Li, F., Shangguan, D., and Ding, Y.: A new global gridded glacier dataset based on the Randolph  
623 Glacier Inventory version 6.0, *Journal of Glaciology*, 67, 773-776,  
624 <https://doi.org/10.1017/jog.2021.28>, 2021.

625 Lüthi, M. P., Bauder, A., and Funk, M.: Volume change reconstruction of Swiss glaciers from length  
626 change data, *Journal of Geophysical Research*, 115, <https://doi.org/10.1029/2010jf001695>, 2010.

627 Machguth, H. and Huss, M.: The length of the world's glaciers – a new approach for the global calculation  
628 of center lines, *The Cryosphere*, 8, 1741-1755, <https://doi.org/10.5194/tc-8-1741-2014>, 2014.

629 Maussion, F., Butenko, A., Champollion, N., Dusch, M., Eis, J., Fourteau, K., Gregor, P., Jarosch, A. H.,  
630 Landmann, J., Oesterle, F., Recinos, B., Rothenpieler, T., Vlug, A., Wild, C. T., and Marzeion, B.:  
631 The Open Global Glacier Model (OGGM) v1.1, *Geoscientific Model Development*, 12, 909-931,  
632 <https://doi.org/10.5194/gmd-12-909-2019>, 2019.

633 Melkonian, A. K., Willis, M. J., and Pritchard, M. E.: Satellite-derived volume loss rates and glacier  
634 speeds for the Juneau Icefield, Alaska, *Journal of Glaciology*, 60, 743-760,  
635 <https://doi.org/10.3189/2014JoG13J181>, 2017.

636 Noel, B., Jakobs, C. L., van Pelt, W. J. J., Lhermitte, S., Wouters, B., Kohler, J., Hagen, J. O., Luks, B.,  
637 Reijmer, C. H., van de Berg, W. J., and van den Broeke, M. R.: Low elevation of Svalbard glaciers  
638 drives high mass loss variability, *Nat Commun*, 11, 4597, [https://doi.org/10.1038/s41467-020-](https://doi.org/10.1038/s41467-020-18356-1)  
639 [18356-1](https://doi.org/10.1038/s41467-020-18356-1), 2020.

640 Oerlemans, J.: A flowline model for Nigardsbreen, Norway: projection of future glacier length based on  
641 dynamic calibration with the historic record, *Annals of Glaciology*, 24, 382-389,  
642 <https://doi.org/10.1017/S0260305500012489> 1997.

643 Pfeffer, W. T., Arendt, A. A., Bliss, A., Bolch, T., Cogley, J. G., Gardner, A. S., Hagen, J.-O., Hock, R.,  
644 Kaser, G., Kienholz, C., Miles, E. S., Moholdt, G., Mölg, N., Paul, F., Radić, V., Rastner, P., Raup,



645 B. H., Rich, J., and Sharp, M. J.: The Randolph Glacier Inventory: a globally complete inventory of  
646 glaciers, *Journal of Glaciology*, 60, 537-552, <https://doi.org/10.3189/2014JoG13J176>, 2014.

647 Pritchard, H. D.: Asia's shrinking glaciers protect large populations from drought stress, *Nature*, 569,  
648 649-654, <https://doi.org/10.1038/s41586-019-1240-1>, 2019.

649 Radić, V. and Hock, R.: Regional and global volumes of glaciers derived from statistical upscaling of  
650 glacier inventory data, *Journal of Geophysical Research*, 115, <https://doi.org/10.1029/2009jf001373>,  
651 2010.

652 RGI Consortium: Randolph Glacier Inventory – A Dataset of Global Glacier Outlines: Version 6.0:  
653 Technical Report, Global Land Ice Measurements from Space, Colorado, USA, 10.7265/N5-RGI-  
654 60, 2017.

655 Scherler, D., Wulf, H., and Gorelick, N.: Global Assessment of Supraglacial Debris-Cover Extents,  
656 *Geophysical Research Letters*, 45, 11,798-711,805, <https://doi.org/10.1029/2018gl080158>, 2018.

657 Schiefer, E., Menounos, B., and Wheate, R.: An inventory and morphometric analysis of British  
658 Columbia glaciers, Canada, *Journal of Glaciology*, volume 54, 551-560, 2008.

659 Shukla, A., Garg, S., Mehta, M., Kumar, V., and Shukla, U. K.: Temporal inventory of glaciers in the  
660 Suru sub-basin, western Himalaya: impacts of regional climate variability, *Earth System Science  
661 Data*, 12, 1245-1265, <https://doi.org/10.5194/essd-12-1245-2020>, 2020.

662 Shukla, T. and Sen, I. S.: Preparing for floods on the Third Pole, *Science*, 372, 232-234,  
663 <https://doi.org/10.1126/science.abh3558>, 2021.

664 Sommer, C., Malz, P., Seehaus, T. C., Lippl, S., Zemp, M., and Braun, M. H.: Rapid glacier retreat and  
665 downwasting throughout the European Alps in the early 21(st) century, *Nat Commun*, 11, 3209,  
666 <https://doi.org/10.1038/s41467-020-16818-0>, 2020.

667 Stuart-Smith, R. F., Roe, G. H., Li, S., and Allen, M. R.: Increased outburst flood hazard from Lake  
668 Palcacocha due to human-induced glacier retreat, *Nature Geoscience*, 14, 85-90,  
669 <https://doi.org/10.1038/s41561-021-00686-4>, 2021.

670 Sugiyama, S., Bauder, A., Zahno, C., and Funk, M.: Evolution of Rhonegletscher, Switzerland, over the  
671 past 125 years and in the future : application of an improved flowline model, *Annals of Glaciology*,  
672 46, 268-274, 2007.

673 Thogersen, K., Gilbert, A., Schuler, T. V., and Malthe-Sorensen, A.: Rate-and-state friction explains  
674 glacier surge propagation, *Nat Commun*, 10, 2823, <https://doi.org/10.1038/s41467-019-10506-4>,  
675 2019.

676 Uemaa, E., Ahi, S., Montibeller, B., Muru, M., and Kmoch, A.: Vertical Accuracy of Freely Available  
677 Global Digital Elevation Models (ASTER, AW3D30, MERIT, TanDEM-X, SRTM, and  
678 NASADEM), *Remote Sensing*, 12, <https://doi.org/10.3390/rs12213482>, 2020.

679 Vargo, L. J., Anderson, B. M., Dadić, R., Horgan, H. J., Mackintosh, A. N., King, A. D., and Lorrey, A.  
680 M.: Anthropogenic warming forces extreme annual glacier mass loss, *Nature Climate Change*, 10,  
681 856-861, <https://doi.org/10.1038/s41558-020-0849-2>, 2020.

682 Winsvold, S. H., Andreassen, L. M., and Kienholz, C.: Glacier area and length changes in Norway from  
683 repeat inventories, *The Cryosphere*, 8, 1885-1903, <https://doi.org/10.5194/tc-8-1885-2014>, 2014.

684 Wu, K., Liu, S., Jiang, Z., Liu, Q., Zhu, Y., Yi, Y., Xie, F., Ahmad Tahir, A., and Saifullah, M.:  
685 Quantification of glacier mass budgets in the Karakoram region of Upper Indus Basin during the  
686 early twenty-first century, *Journal of Hydrology*, 603,  
687 <https://doi.org/10.1016/j.jhydrol.2021.127095>, 2021.

688 Xia, W.: An Automatic Extraction Method of Glacier Length Based on Voronoi Algorithm - A Pilot Study

689 in the Sanjiangyuan Region, College of Urban and Environmental Science, Northwest University,  
690 Xi'an, Shannxi, 2020.

691 Yang, B. Y., Zhang, L. X., Gao, Y., Xiang, Y., Mou, N. X., and Suo, L. D. B.: An integrated method of  
692 glacier length extraction based on Gaofen satellite data, *Journal of Glaciology and Geocryology*, 38,  
693 1615-1623, <https://doi.org/10.7522/j.issn.1000-0240.2016.0189>, 2016.

694 Yao, X. J., Liu, S. Y., Zhu, Y., Gong, P., An, L. N., and Li, X. F.: Design and implementation of an  
695 automatic method for deriving glacier centerlines based on GIS, *Journal of Glaciology and*  
696 *Geocryology*, 37, 1563-1570, <https://doi.org/10.7522/j.issn.1000-0240.2015.0173>, 2015.

697 Zemp, M., Huss, M., Thibert, E., Eckert, N., McNabb, R., Huber, J., Barandun, M., Machguth, H.,  
698 Nussbaumer, S. U., Gartner-Roer, I., Thomson, L., Paul, F., Maussion, F., Kutuzov, S., and Cogley,  
699 J. G.: Global glacier mass changes and their contributions to sea-level rise from 1961 to 2016,  
700 *Nature*, 568, 382-386, <https://doi.org/10.1038/s41586-019-1071-0>, 2019.

701 Zhang, D. and Zhang, S.: A new global dataset of mountain glacier centerline and length, *Science Data*  
702 *Bank*, <https://doi.org/10.11922/sciencedb.01643>, 2022.

703 Zhang, D., Yao, X., Duan, H., Liu, S., Guo, W., Sun, M., and Li, D.: A new automatic approach for  
704 extracting glacier centerlines based on Euclidean allocation, *The Cryosphere*, 15, 1955-1973,  
705 <https://doi.org/10.5194/tc-15-1955-2021>, 2021.

706 Zheng, G., Allen, S. K., Bao, A., Ballesteros-Cánovas, J. A., Huss, M., Zhang, G., Li, J., Yuan, Y., Jiang,  
707 L., Yu, T., Chen, W., and Stoffel, M.: Increasing risk of glacial lake outburst floods from future Third  
708 Pole deglaciation, *Nature Climate Change*, 11, 411-417, [https://doi.org/10.1038/s41558-021-01028-](https://doi.org/10.1038/s41558-021-01028-3)  
709 [3](https://doi.org/10.1038/s41558-021-01028-3), 2021.

710 Zhou, S., Yao, X., Zhang, D., Zhang, Y., Liu, S., and Min, Y.: Remote Sensing Monitoring of Advancing  
711 and Surging Glaciers in the Tien Shan, 1990–2019, *Remote Sensing*, 13,  
712 <https://doi.org/10.3390/rs13101973>, 2021a.

713 Zhou, Y., Li, X., Zheng, D., Li, Z., An, B., Wang, Y., Jiang, D., Su, J., and Cao, B.: The joint driving  
714 effects of climate and weather changes caused the Chamoli glacier-rock avalanche in the high  
715 altitudes of the India Himalaya, *Science China Earth Sciences*, 64, 1909-1921,  
716 <https://doi.org/10.1007/s11430-021-9844-0>, 2021b.

717